Computers and Geotechnics 125 (2020) 103656

Contents lists available at ScienceDirect

Computers and Geotechnics

journal homepage: www.elsevier.com/locate/compgeo

Research Paper

Strategies for numerical simulation of cast-in-place piles under axial loading

Christoph Schmüdderich[a], Mohammad Mahdi Shahrabi[c,1], Mahdi Taiebat[b], Arash Alimardani Lavasan[a,*]

[a] Chair of Soil Mechanics, Foundation Engineering and Environmental Geotechnics, Ruhr-Universität Bochum, Germany
[b] Department of Civil Engineering, University of British Columbia, Vancouver, Canada
[c] Golder Associates Inc., Vancouver, Canada

ARTICLE INFO

Keywords:
Full-displacement piles
Expander body
Sensitivity analysis
In situ tests
HSS model parameter estimation
Back analysis

ABSTRACT

Pile foundations are constructed using a variety of installation methods, which can significantly influence their behavior under axial loading. In this study, numerical simulations of a bored pile, a full-displacement pile and a full-displacement pile with attached expander body have been carried out using standard finite-element analysis where constitutive model parameters are estimated based on various geotechnical field measurements. Considering variations of in situ test measurements, conservative, best estimate and optimistic sets of the calibrated model parameters have been used for the subsurface soil. In order to capture the effect of pile installation method, different numerical strategies have been examined and their applicability to each of the installation methods evaluated. By studying the load-movement response and load distributions along the pile under head-down loading tests, results of the numerical simulations have been evaluated and compared to those obtained from a monitored field study. Finally, local and global sensitivity analyses, as well as a parameter identification procedure have been, respectively, used to find out the most contributing model parameters and to improve model predictions. Results of the numerical simulations signify the importance of a verified staged procedure for modeling the bored and full-displacement piles, as well as the expander body to best capture the pile bearing capacity and load-movement behavior. Furthermore, the parametric study undertaken reveals that acceptable predictions can only be achieved if the most contributing model parameters are identified and calibrated adequately.

1. Introduction

Pile foundations are among the classical foundation types in geotechnical engineering and are of particular interest in grounds where the surficial layers are dominated by loose or soft soils. Since their design is dependent on the performance of structures built on top of them, an adequate prediction of the pile load-movement behavior is of great importance. One way of categorizing pile foundations is based on their installation method and the corresponding displacements imposed to the surrounding soil during the installation process. In general, three categories can be defined: non-displacement piles (e.g., bored piles, drilled shafts), partial displacement piles (e.g., H piles, continuous flight auger piles) and full-displacement piles (FDP, e.g., drilled displacement piles, precast concrete piles). A further distinction between the partial and full-displacement piles is reasonable in terms of their installation procedure (e.g., driving, drilling) which is linked to the type of the pile structure (e.g., precast, cast-in-place). A key aspect for reliable prediction of the axial bearing capacity of piles for design purposes is to understand how the installation method influences the stress states in the surrounding soil. In contrast to non-displacement piles and in particular those constructed using casings where installation effects are relatively inconsiderable, the increase in bearing capacity due to FDP installation method is significant and thus, should be taken into account. However, since the imposed displacements alter the stress state and density of the soil in proximity of the pile, which in turn are affected by the soil type, initial stress state, the pile or drilling tool geometry, and the driving or drilling speed, an advanced design method that accounts for these aspects is required. Additionally, the manner in which a given design method is influenced by each of these aspects has to be clearly identified and investigated for meaningful design.

Over the past decades, several analytical design methods for driven piles in different types of soil have been proposed, including but not limited to those presented by Jardine et al. (2005) (ICP design method), Lehane et al. (2005) (UWA-05 method) and Karlsrud et al. (2005) (NGI approach). A detailed review of various analytical design methods has been published by Niazi and Mayne (2013). Parametric studies and

* Corresponding author.
E-mail address: arash.alimardanilavasan@rub.de (A. Alimardani Lavasan).
[1] Formerly, Department of Civil Engineering, University of British Columbia.

https://doi.org/10.1016/j.compgeo.2020.103656
Received 18 October 2019; Received in revised form 11 May 2020; Accepted 11 May 2020

further comparison between analytical design methods have also been conducted by Xu et al. (2008) and Labenski and Moormann (2016) among the others. However, analytical methods mostly apply for specific soil types and may not apply to mixed soils and multi-layered soil strata.

In addition to the analytical design methods for driven piles, several studies have been performed on this subject using numerical simulations, for instance those by Pucker and Grabe (2012), Hamann et al. (2015) and Ko et al. (2016) using Coupled Eulerian–Lagrangian (CEL) method, by Dijkstra et al. (2011) and Rooz and Hamidi (2019) using Arbitrary Lagrangian–Eulerian (ALE) method and by Phuong et al. (2016) and Lorenzo et al. (2017) using Material Point method (MPM).

Although a large-strain solution best resembles the installation process for full-displacement piles, several studies have been conducted adopting standard finite-element analysis. Employing a standard finite element code for such problems requires some simplifying assumptions to address the evolution of stress state around the pile and to mimic the state variation induced in the ground during the installation. Since the displacement tool increases horizontal stresses due to lateral movements in the soil, assumptions should be made in numerical models to address such effect leading to higher shaft friction. This effect can be simulated by applying volume expansion, radial displacement, or radial stresses exchange due to the pile installation. In the past decade, several attempts have been made to approximate the FDP installation effects, for instance, by Said et al. (2009),Krasiński (2014) and Engin et al. (2015). However, these approaches have only been studied and discussed independent from one another, validated for their specific cases of study and not compared to other approaches.

In cases where the pile shaft and tip do not provide sufficient bearing capacity to carry high service loads, base resistance can be significantly increased by attaching an Expander Body (EB) to the pile toe. Although EBs have been used for decades and empirical design methods have been proposed (Berggren et al., 1998;Report; Massarsch and Wetterling, 1993; Terceros et al., 1995), an adequate numerical approach to simulation of their installation and inflation processes has not been investigated intensively. Therefore, an appropriate method to numerically predict the increased bearing capacity of EB-enabled piles is still in debate.

To accurately predict the system response, an adequate numerical model in conjunction with appropriate constitutive parameters has to be adopted. Therefore, inaccuracies associated with numerical models may be related to the simulation technique, as well as to uncertainties of the constitutive parameters. In this study, both uncertainties are attempted to be taken into account for numerical modeling of various pile types tested at the Bolivian Experimental Site for Testing (BEST) piles (Fellenius and Terceros, 2017). While different modeling scenarios are undertaken herein to produce a numerical technique capable of properly simulating field test results, uncertainties associated with soil parameters at the site are accounted for by defining ranges spanning the conservative, average and optimistic parameter sets. Furthermore, a detailed investigation is necessary to better understand the influence of individual input parameters on the outputs of the numerical model. The importance of such investigation becomes more evident by knowing that soil parameters are obtained based on empirical correlations which typically takes into account neither the nature of geotechnical application nor the anatomy of the constitutive model. For this reason, sensitivity analysis can be used to determine soil parameters with significant influence on the model output (Sobol, 1993; Saltelli et al., 2008; Miro et al., 2014). Furthermore, inverse analysis (Sakurai et al., 2003; Yazdani et al., 2012; Knabe et al., 2012; Zhao et al., 2015) can be performed to identify the values of uncertain parameters using measurements from field investigations and in situ load tests.

This paper aims to compare different numerical approaches available in the literature to demonstrate if they are able to capture the installation process of full-displacement piles, to introduce numerical simulation approaches for expander bodies and to analyze whether constitutive parameters derived from empirical correlations can serve as the basis for numerical simulation of pile load tests. In order to achieve that, the reported filed test measurements from the BEST are considered as the benchmark.

2. Bolivian experimental site for testing piles

2.1. General site conditions and geotechnical investigation program

As a part of the comprehensive pile testing program adopted by ISSMGE's TC-212, a geotechnical site investigation program was carried out prior to various piles being constructed, instrumented, loaded and monitored at the Bolivian Experimental Site for Testing piles (BEST) in Santa Cruz, Bolivia (Fellenius and Terceros, 2017). The geotechnical site investigation included piezo-Cone Penetration Test (CPTu), and both regular and Seismic Flat Dilatometer Test (DMT/SDMT). Index measurements, as well as disturbed samples taken at the site over a depth of approximately 16 m were used to identify 5 soil layers, as further discussed in Fellenius and Terceros (2017), and to estimate initial state and constitutive model parameters associated with each layer by taking advantage of conventional index-based empirical correlations.

The 3 pile tests at the BEST which are of interest in this paper were linearly located over a distance of approximately 55 m (Fig. 1). The four locations at which the geotechnical investigations presented in Figs. 2 and 3 were carried out, were all along the line connecting these 3 test piles. Therefore, it is assumed that the soil layering and parameters, used herein for the purpose of numerical modeling, do not vary significantly at the location of each individual pile and that the average index values of the 4 field tests of the same type (e.g., CPTu) are valid for the entire site.

As described in Fellenius and Terceros (2017), the geology of the site is dominated by fine to medium silty sand with intermittent layers of clay and clayey sand. The subsurface layering profile obtained from the analysis of CPTu and DMT index measurements were found to be comparable with the reported soil logs obtained from borehole samples taken every 1 m. The subsoil profile was therefore divided into a layer of medium to dense silty sand at 0–2 m depth (L1), underlain by clay at 2–3 m depth (L2), very loose silty sand at 3–6 m depth (L3), loose to medium dense silty sand at depth 6–12 m (L4), and clay at lower depths

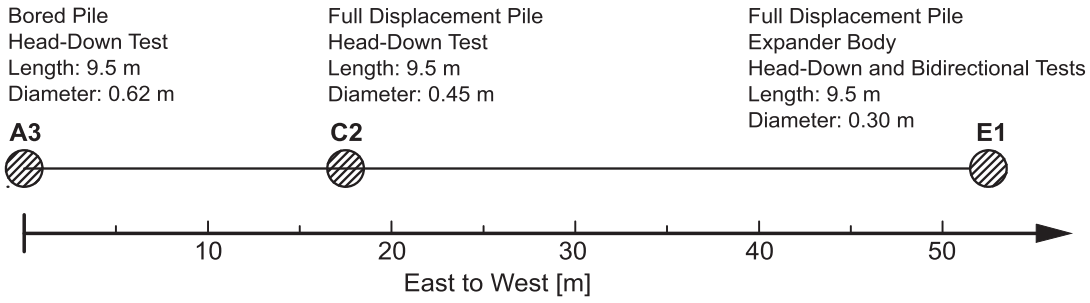

Fig. 1. Layout of test piles at the BEST used for numerical simulations.

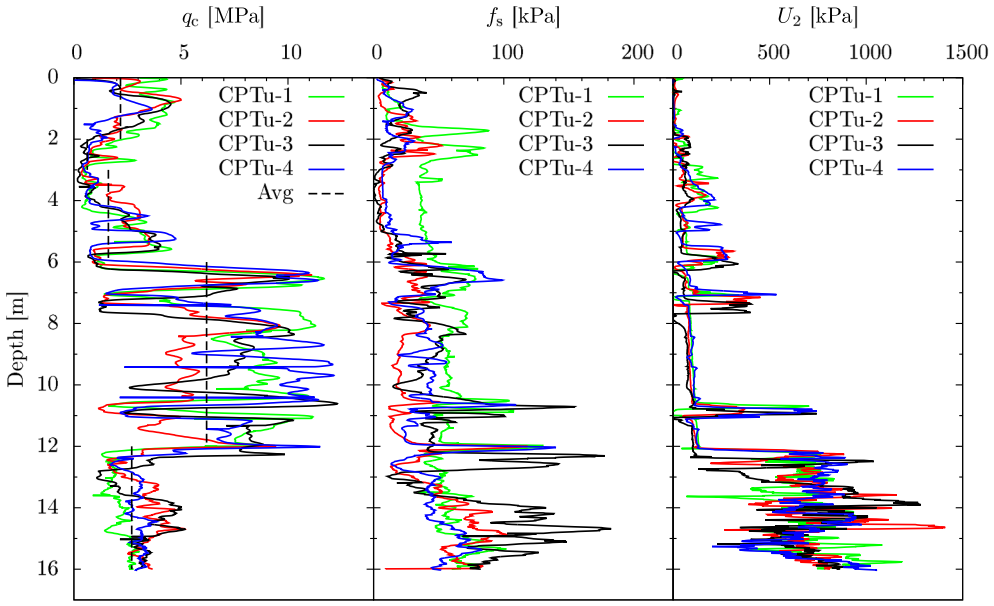

Fig. 2. Overlay plots of CPTu profiles of cone resistance, sleeve friction, and pore pressure.

up to 16 m (L5). Due to seasonal influences, the water table was reported to vary between the ground surface and 2–3 m depth. Thus, at the time when the field investigations were conducted it was observed that the water table was at approximately 2 m depth, whereas it was very close to the ground surface when the piles were installed and tested (Fellenius and Terceros, 2017). For boundary value simulations discussed later in this paper, the groundwater table has been assumed to be at the ground surface.

2.2. Test piles

The pile testing program at the BEST involved 13 cast-in-place single piles drilled and installed using various techniques including boring by conventional auger, boring by the Continuous Flight Auger (CFA), and the Full Displacement Pile (FDP) tool, some of which were also equipped with Expander Body (EB) and post grouting at the pile toe. Fig. 4(a) - (d) depicts the main drilling tools used at the site for construction of the piles. Furthermore, Fig. 4(e) schematically depicts how an inflated EB attached below a pile looks like and how it contributes to the pile bearing capacity.

A total of 26 static and 4 dynamic tests were also carried out on the piles, for some of which the results were provided to the participants in a prediction event. Based on the data provided, the focus of the present paper is on numerical simulation of three piles under static loading: a bored pile drilled with slurry (A3), an FDP (C2), and an FDP equipped with an EB (E1). Fig. 1 shows relative locations of the piles understudy

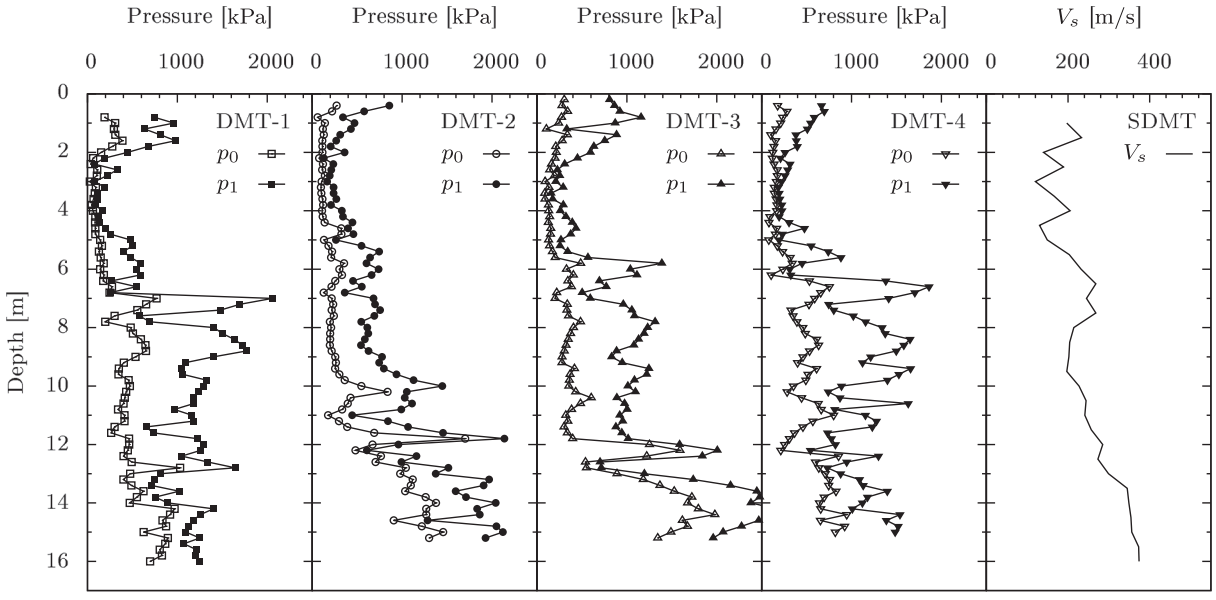

Fig. 3. DMT and SDMT profiles of p_0, p_1, and V_s measured at the BEST.

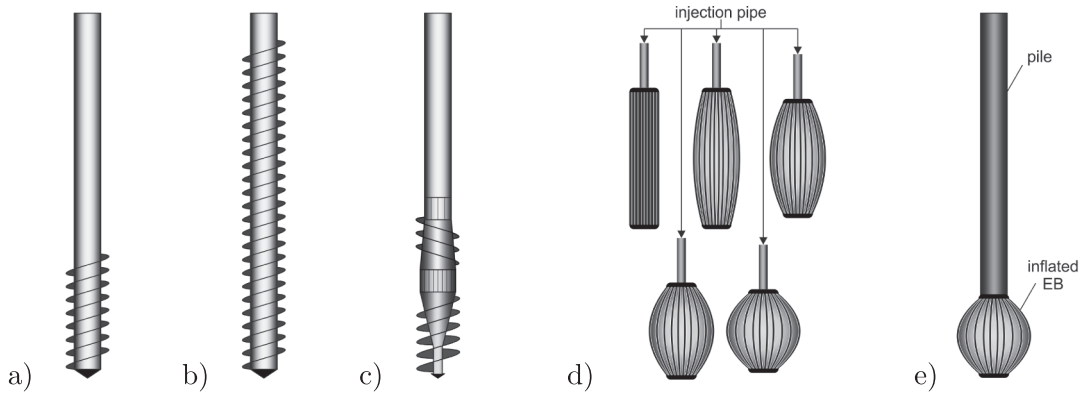

Fig. 4. Drilling tools used for pile construction at the BEST, (a) conventional boring auger, (b) Continuous Flight Auger (CFA), (c) Full Displacement Pile (FDP) installation tool, (d) Expander Body (EB), (e) Concreted pile with attached Expander Body after inflation process.

at the BEST, and summarizes relative characteristics of each one. All test piles were installed to 9.5 m depth (bottom of reinforcement cage) below the ground surface and varied in diameter as A3, C2, and E1 were constructed with 620 mm, 450 mm, and 300 mm diameter casings, respectively. The EB unit installed at the toe of E1 was reportedly expanded to an approximate size of 1 m in length and 0.4 m in width. Static head-down loading tests were performed on all piles and strain gauges at 2.0 m, 5.0 m, and 7.5 m depths were used to capture the distribution of loads along the piles. A bidirectional loading cell was also installed on E1 at 8.3 m depth. However, due to the expansion of the EB, the connection of one telltale on the bidirectional cell to the pile was broken, and the recorded data was not found to be interpretable. Hence, the results of head-down tests on E1 were also used herein for numerical simulations.

3. Numerical simulation

3.1. Description of the model

In the present study, boundary value simulations of different pile installation scenarios, as well as head-down loading tests are carried out in a widely used finite element (FE) software, Plaxis 2D, under axisymmetric geometry and loading conditions. Regardless of the numerical simulation stages adopted for different pile installation techniques, the initial stress field is defined using the K_0-procedure, which is reasonable given the simple geometry of the model. In the numerical simulations carried out in the present study, the aspects such as the infiltration of the concrete into the surrounding soil, the micro/meso scale interactions at the contact between the pile and soil, and the water flow due to the excavation and pile installation have not been considered. The details of method that has been adopted to simulate the contact between the pile and the surrounding soil will be introduced in the following sections. Based on results obtained from trial simulations, the size of the model domain has been selected such that boundary effects are avoided. Accordingly, the width and height of the model are 15 m and 20 m equal to approximately 24 and 2 times the pile diameter and length, respectively [Fig. 5(a)]. As shown in Fig. 5(b), the model domain is discretized using a total number of 3424 15-node triangular elements. In order to minimize approximations associated with the discretization of the model in FE analysis, the mesh is refined inside the pile structure, within a primary zone of 3*D* and a secondary zone of 5*D* below the tip and beside the shaft, *D* being the pile diameter. The mesh size is gradually increased towards the model boundaries to minimize the computational effort, while it is ensured that results remain irrespective of the increased mesh size. A magnified view of the 2D mesh configuration in the proximity of the pile shaft and tip is shown in Fig. 5(c). To realistically capture the soil-pile interaction, and to avoid stress concentrations at the corner of the pile tip, interface elements are introduced at soil-pile contacts, extending 0.5 m vertically and horizontally from the corner of the pile tip into Layer 4 [Fig. 5(c)]. The preliminary analyses revealed that the excess pore water pressure induced by the pile installation process would dissipate within less than one day. Since the pile loading in the field was carried out a few weeks after the installation, the numerical analyses were conducted in accordance with drained condition.

3.2. Constitutive model and parameter estimation for soils and interfaces

An important component of any numerical simulation is adopting a proper constitutive model that is capable of effectively simulating complex stress–strain behavior. The stress dependency of stiffness plays a significant role in models where the variation of geo-static stresses is considerable (e.g., tunnels, deep excavations, and foundations). In addition and specific to this study, as the pile may undergo a wide range of strains during installation and loading, the constitutive model should also capture the degradation of shear modulus with the evolution of shear strain. Lastly, the constitutive model should account for gradual mobilization of the shear strength in the soil during plastic flow. With reference to all these critical modeling aspects, the Hardening Soil with Small-strain overlay (HSS) model (Benz et al., 2009), which is an extension of the Hardening Soil (HS) model (Schanz et al., 1999), is adopted in the present study as an adequate constitutive model.

As discussed in Section 2.1, the subsurface soil strata at the BEST consisted primarily of various layers of silty sand and clay, for which HSS model parameters had to be separately calibrated. At the preliminary stage of this study, an extensive research was done on empirical correlations available in the geotechnical literature based on different types of in situ testing carried out at the BEST to come up with a unified approach for estimation of HSS model parameters.

Conventionally, standard and advanced laboratory tests, namely triaxial and oedometer tests as well as bender element and resonant column tests, are required to properly calibrate HSS model's stiffness, shear strength, and small strain parameters (Benz, 2007). In practice, however, the use of such tests is very limited due to the difficulties in soil sampling and complications in laboratory testing, and in situ index tests such as SPT, CPT and DMT are rather preferred. The results of these field tests are influenced by the material properties and also by the corresponding boundary conditions. Therefore, it is not possible to directly calibrate all model parameters using these field tests, because of the inherent boundary value problem nature of these test. As a consequence, it is common practice to obtain primary model parameters using well-established empirical correlations and select the secondary ones using simplifying assumptions.

Herein, six HSS model parameters are grouped into the primary parameters category. The compression stiffness for primary loading, E_{oed}, the peak friction angle, ϕ'_p, the maximum dilation angle, ψ_{max}, the

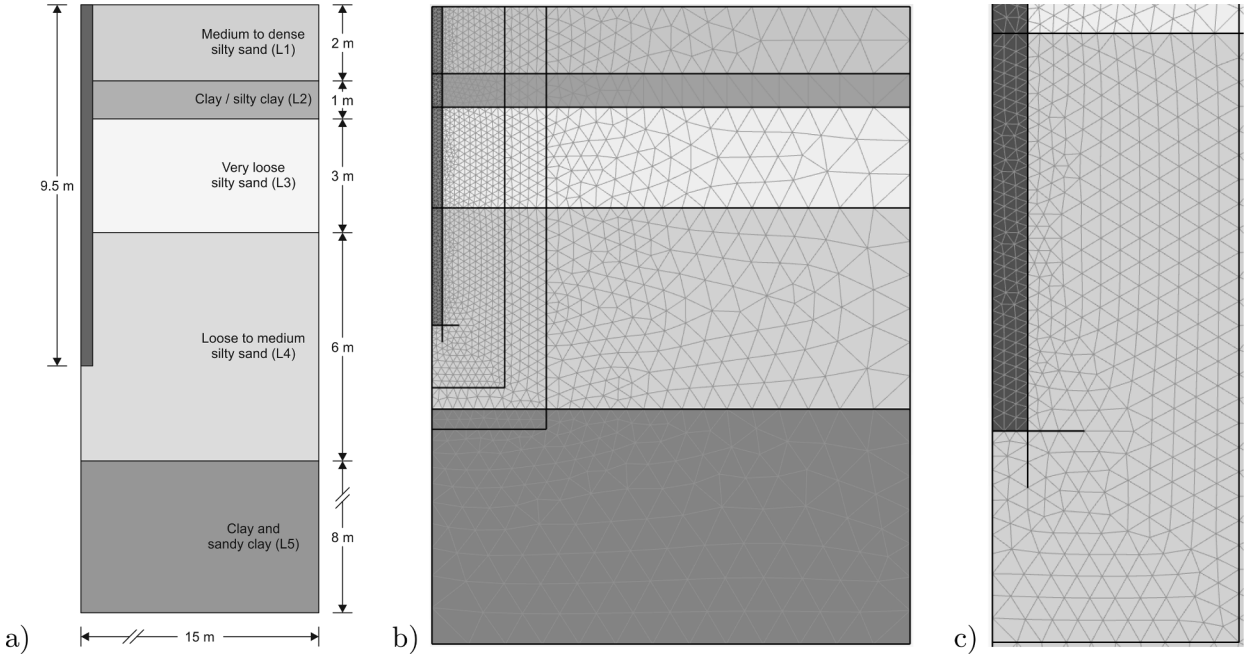

Fig. 5. (a) Model geometry, (b) discretization of 2D axisymmetric FE model, (c) magnified view of the mesh in proximity of the pile shaft and tip.

threshold shear strain for stiffness degradation, $\gamma_{0.7}$ and the coefficient of lateral earth pressure, K_0, are estimated using empirical correlations, while the small strain stiffness, G_0, is calculated by direct measurement of the shear wave velocity, v_s, as carried by means a seismic test (SDMT in this study). Table 1 summarizes the correlations undertaken for estimation of the primary parameters for each of the identified soil layers at the BEST. It is to be noted that ψ_{max} (conservative, average and optimistic values) has been assumed to be zero for very loose sand and clay layers (i.e., L2, L3, and L5) while the HSS-specific model parameter, $\gamma_{0.7}$, has been suggested in the literature to range between 1×10^{-4} and 2×10^{-4} (Benz, 2007).

Other HSS model parameters (E_{50}^{ref}, E_{ur}^{ref}, m) have been obtained using simplified assumptions suggested by Benz (2007). One of these parameters is the stiffness power law exponent, m, which is used to normalize the stiffness moduli at the reference confining pressure, p_{ref}. The m value, ranging between 0.5 to 1.0 respectively for dense/stiff to loose/soft soils, is assumed to be equal to 0.5, 0.9, 0.7, 0.5 and 0.8 for L1 to L5, respectively, to transform the stiffness values from in situ stress into reference pressure E_{oed}^{ref} and G_0^{ref}. Other stiffness parameters, namely the confining stress dependent stiffness modulus for primary loading, E_{50}^{ref}, and the unloading/reloading stiffness E_{ur}^{ref}, are estimated using the following assumptions: $E_{50}^{ref}/E_{oed}^{ref} = 1.0$ for sand, $E_{50}^{ref}/E_{oed}^{ref} = 1.25$ for clay, $E_{ur}^{ref}/E_{oed}^{ref} = 3.0$ for medium to dense sand, $E_{ur}^{ref}/E_{oed}^{ref} = 4.0$ for loose sand, and $E_{ur}^{ref}/E_{oed}^{ref} = 5.0$ for clay.

The results reported from the field tests (Figs. 2 and 3) carried out at 4 different locations along the line connecting test piles A3 and E1 (Fig. 1) have been used to determine the average model parameters for each layer (i.e., L1 to L5), as well as the average plus and minus one standard deviation as a measure of the confidence intervals for variation of each parameter within a given layer. In the context of this paper, these sets of parameters are referred to as the average, optimistic, and conservative sets, which are summarized in Table 2.

To address the possibility of gap opening/closure normal to the soil-pile contact as well as relative displacement and plastic slip parallel to

Table 1
The proposed approach to estimation of HSS model parameters.

Parameter	Estimation approach/correlation	Reference
E_{oed}^{ref}	$E_{oed} = R_M E_{DMT}$ $R_M = 0.14 + 2.36\log K_{DMT} \geqslant 0.85$ for $(I_{DMT} \leq 0.6)$ $R_M = R_{M,0} + (2.5 - R_{M,0})\log K_D \geqslant 0.85$ for $(0.6 < I_{DMT} < 3)$ with $R_{M,0} = 0.14 + 0.15(I_{DMT} - 0.6)$ $R_M = 0.5 + 2\log K_{DMT} \geqslant 0.85$ for $(I_{DMT} \geqslant 3)$ $R_M = 0.32 + 2.18\log K_{DMT} \geqslant 0.85$ for $(I_{DMT} > 10)$	Marchetti et al. (2001)
K_0	$K_0 = \begin{cases} 0.376 + 0.095K_{DMT} - 0.0017\frac{q_c}{\sigma'_{v0}}, & \text{for sand} \\ (K_{DMT}/1.5)^{0.47} - 0.6, & \text{for clay} \end{cases}$	Marchetti (1980),Baldi et al. (1986)
ϕ'_p	$\phi'_p = 15.575\left(\frac{q_c}{\sigma'_{h0}}\right)^{0.1714}$	Lee et al. (2004)
ψ_{max}	$\phi'_p - \phi'_{cv} \simeq 0.4\psi_{max} = 3 \cdot I_R$	Bolton (1986)
	$I_{R,CPT} = \frac{1}{3.1}\ln\left[\frac{q_c/p_a}{17.68(\sigma'_{v0}/p_a)^{0.5}}\right]\left[12.1 - \ln\left(\frac{100q_c}{p_a}\right)\right] - 0.12$	Jamiolkowski et al. (2001), Lee et al. (2008)
G_0^{ref}	$G_0 = \rho v_s^2$	Seismic tests(SDMT in this study)
$\gamma_{0.7}$	$\gamma_{0.7} = \frac{0.385}{4G_0}[2c\left(1 + \cos 2\phi'_p\right) + \sigma'_{v0}\left(1 + K_0\right)\sin 2\phi'_p]$	Benz (2007)

Table 2
Initial stress and estimated model parameters for the BEST.

	Parameter	γ_{sat}	ϕ'_p	ψ_{max}	E_{oed}^{ref}	E_{50}^{ref}	E_{ur}^{ref}	m	G_0^{ref}	$\gamma_{0.7}$	K_0
	Unit	[kN/m^3]	[°]	[°]	[MPa]	[MPa]	[MPa]	[-]	[MPa]	[-]	[-]
	conservative		34.5	9.2	24.3	24.3	72.9		218.5	1.0E-4	0.33
L1*	average	19.0	37.7	12.6	41.1	41.1	123.3	0.5	225.3	1.0E-4	0.66
	optimistic		40.9	15.9	57.8	57.8	173.4		232.1	1.6E-4	0.99
	conservative		24.0		2.8	3.5	17.5		51.0	1.1E-4	0.50
L2*	average	16.0	26.0	0.0	4.8	6.0	30.0	0.9	93.4	1.9E-4	0.76
	optimistic		28.0		6.7	8.3	41.8		135.7	2.0E-4	1.03
	conservative		28.2		4.1	4.1	16.4		62.4	1.0E-4	0.32
L3*	average	16.0	31.7	0.0	9.4	9.4	37.6	0.7	103.3	1.5E-4	0.48
	optimistic		36.2		14.7	14.7	58.8		135.7	2.0E-4	0.63
	conservative		33.7	9.4	12.9	12.9	38.7		122.6	1.0E-4	0.30
L4*	average	19.0	37.4	10.6	26.4	26.4	79.2	0.5	159.1	1.3E-4	0.42
	optimistic		41.8	11.7	39.8	39.8	119.4		195.6	1.6E-4	0.63
	conservative		28.0		8.5	10.6	53.1		108.5	1.2E-4	0.85
L5*	average	18.0	30.0	0.0	14.5	18.1	90.6	0.8	123.7	1.4E-4	1.28
	optimistic		32.0		20.6	25.7	128.8		138.8	1.6E-4	1.72

* constant model parameters: $c = 0\,\text{kPa}$, $p_{ref} = 100\,\text{kPa}$, $\nu_{ur} = 0.2$, $R_f = 0.9$

the contact, an elastoplastic interface element has been adopted in the intermediate contact between the pile and soil. In this interface, the elastic normal behavior (normal displacements with no interpenetration) reads the oedometric stiffness (E_{oed}) while the elastic shear behavior (tangential displacement) is governed by the shear stiffness (G). When the interface tensile strength (σ_t) or shear strength $\tau = c_{int} + \sigma_n \tan\delta$ (where σ_n is the normal stress and c_{int} and δ refer to interface cohesion/adhesion and friction angle) is reached, gap opening in normal direction or plastic slip in tangential direction may occur, respectively. To set the interface properties, a complete set of parameters with identical stiffness as the surrounding soil and reduced shear strength ($\delta / \phi' = 0.67$ for bored pile, $\delta / \phi' = 0.9$ for FDP, $\delta / \phi' = 1.0$ for EB) is adopted to the interface in this study. Apparently, this approach for the simulation of the pile-soil interface neglects the impact of micro/meso asperities as is the case for the pile-rock contact (Johnston and Lam, 1989).

3.3. Modeling approach for numerical simulation of the bored pile

As described in Wehnert and Vermeer (2004) and Han et al. (2017), the modeling approach adopted to simulate the construction and loading process of a bored pile, such as pile A3, can be summarized as follows: In the initial phase, geo-static stresses are initialized using the K_0-procedure. In the excavation phase, the soil volume is removed while support at the walls and the bottom is assumed in the normal direction. In the pile casting phase, the pile volume is activated and concrete material assigned. Furthermore, interface elements are activated to enable realistic pile-soil interaction. Finally, in the loading phase, a displacement controlled head-down loading test is performed. The phases used are also schematically demonstrated in Fig. 6 in a more accessible way. In this study, the stiffness of the pile is considered significantly higher than the stiffness of the surrounding soil. Therefore, linear elastic behavior is assumed for the pile made of stiff concrete. The concrete material parameters assigned are a unit weight of $\gamma = 24\,\text{kN/m}^3$, a Poisson's ratio of $\nu = 0.2$ and a Young's modulus of $E = 2.5{\cdot}10^7\,\text{kN/m}^2$. Despite the possible variation of the concrete properties (due to improper concreting), this research assumes homogeneous concrete piles with low toleration in the unit weight and the stiffness of the concrete.

3.4. Modeling approaches for numerical simulation of FDP

Pile installation effects due to considerable variation of stresses in the soil surrounding the pile have brought about complexities in understanding and modeling of FDPs. Nonetheless, there are several numerical and empirical methods in the literature which have taken into account the interaction and stress changes during the installation of these pile types to predict their capacity. In the present study, four different simulation approaches for FDP are investigated and tested against the results from field tests at the BEST. Within this paper, these approaches are referred to as Mixed Empirical-Numerical (MEN) (Said et al., 2009), Cavity Expansion (CE) (Krasiński, 2014), Cavity Expansion with Sub-Layering (CE-SL) and Cavity Expansion with Vertical Shearing (CE-VS). Detailed information about these approaches, which are also graphically shown in Fig. 7 is given in the following sections. A comparison of these approaches with load test measurements from BEST is presented in Section 4.2.

3.4.1. Mixed Empirical-Numerical (MEN) approach

To account for the installation process of displacement piles, Said et al. (2009) proposed a numerical method, here referred to as Mixed Empirical-Numerical (MEN) approach. Although the MEN approach has been proposed for sandy soils, the idea here is to investigate whether the approach can be applied to the current test field at BEST, which is characterized by silty sands with intermittent layers of clay and clayey sand. In general, Said et al. (2009) considered three phases for the installation process [Fig. 7(a)]. After initiation of geo-static stresses according to the K_0-procedure, the soil volume in place of which the pile is installed, is removed and stress changes due to FDP installation are applied before the pile is cast in place. Finally, the static head-down loading test is simulated by a displacement controlled boundary condition gradually being applied on the pile head.

To take into account the pile installation effects, the radial pressure, σ'_{rc}, and shear stress in the upward direction, τ_{res}, denoted as the negative residual friction, are applied at the pile shaft. Additionally, the residual base pressure, q_{p-res}, is applied at the pile tip. σ'_{rc} and q_{p-res} are determined based on empirical equations, whereas τ_{res} is calculated from the equilibrium of vertical forces. It has to be noted that these empirical equations have mainly been developed for clean sands and not for soils containing large silt fractions.

To estimate σ'_{rc}, Said et al. (2009) suggested to employ the Imperial College Pile (ICP) design method introduced by Chow (1997) and Jardine et al. (2005), which has been further validated in other studies (Jardine et al., 2006; Jardine et al., 2015). According to the ICP design method, σ'_{rc} at a given depth of z is calculated by

$$\sigma'_{rc} = 0.029\, q_c \left(\frac{\sigma'_v}{p_a}\right)^{0.13} \left(\frac{h}{R}\right)^{-0.38} \tag{1}$$

where q_c is the tip resistance from the conventional Cone Penetration Test (CPT), σ'_v is the effective vertical stress at the z depth, p_a is the

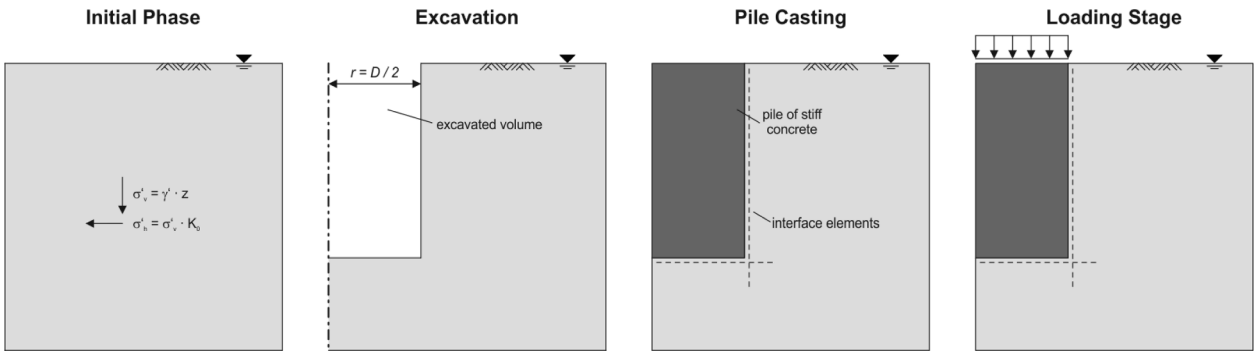

Fig. 6. Construction and subsequent static head-down loading phases adopted for the numerical simulation of bored piles with axisymmetric geometry and boundary conditions.

atmospheric pressure typically assumed to be 100 kPa, h is the distance from the z depth to the pile tip, and R is the pile radius. To avoid stress concentrations at the pile tip, h/R should not be smaller than 8 (Jardine et al., 2005).

According to Said et al. (2009), q_{p-res} (kPa) is calculated as the mean value of two empirical equations. The first equation introduced by Briaud and Tucker (1984) is given as

$$q_{p-res} = 533.4 L \beta \quad (2)$$

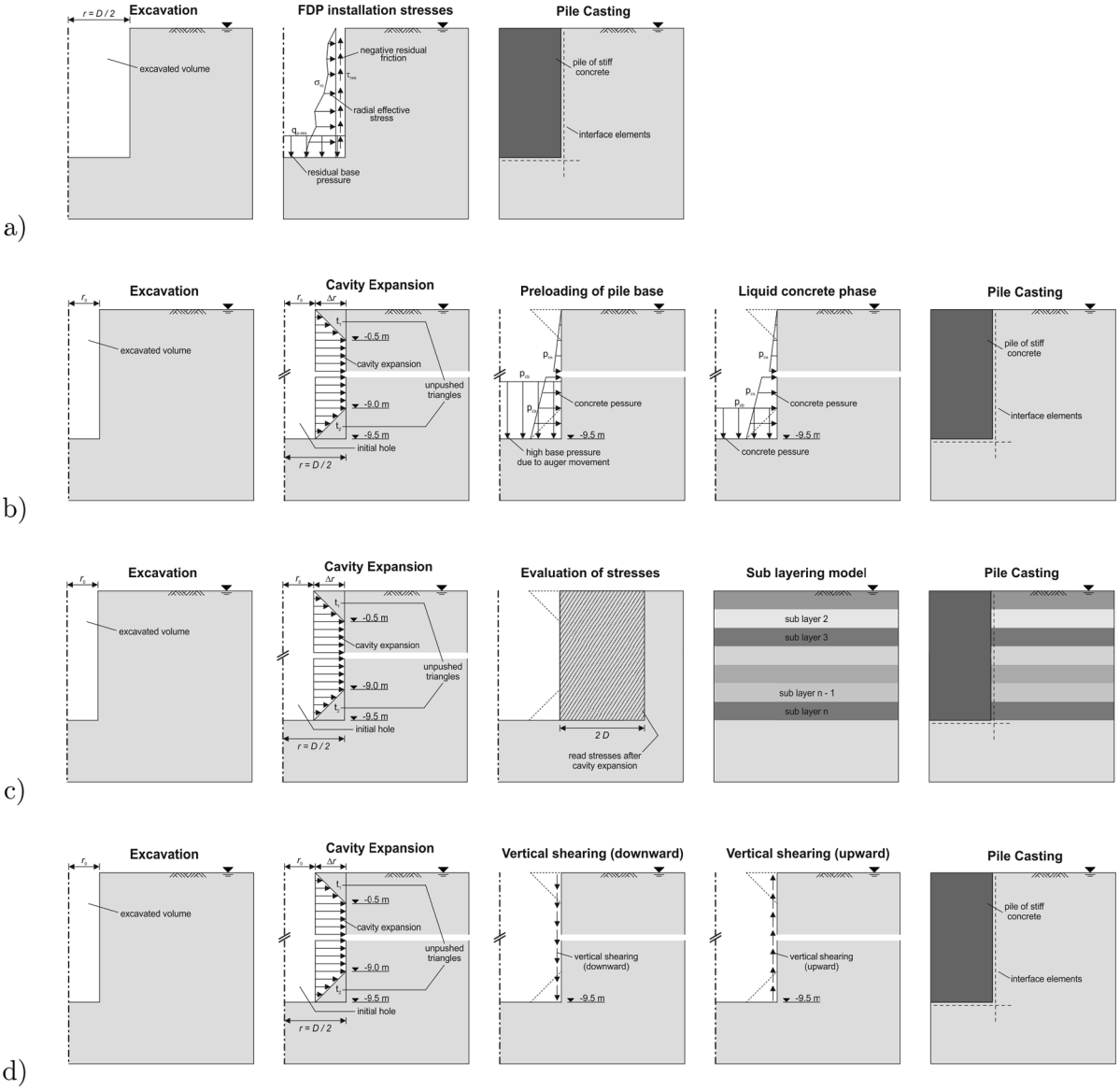

Fig. 7. Installation stages for numerical simulation of FDP: (a) Mixed Empirical-Numerical (MEN) approach, (b) Cavity Expansion (CE) approach, (c) Cavity Expansion with Sub-Layering (CE-SL) approach, and (d) Cavity Expansion with Vertical Shearing (CE-VS) approach.

where L is the pile length (m), and

$$\beta = \sqrt{\frac{K_\tau P}{A E_p}} \tag{3}$$

where P is the pile perimeter (cm), A is the pile area (m^2), E_p is the elastic modulus of the pile (kPa), and K_τ (kPa/cm) is referred to as the initial slope of the friction curve during loading (kPa/cm) defined as

$$K_\tau = 188.9(N_{side})^{0.27} \tag{4}$$

where N_{side} is the average Standard Penetration Test (SPT) blow count number around the pile tip. The second equation is given by Alawneh and Malkawi (2000) as

$$q_{p-res} = 13158\eta^{0.724} \tag{5}$$

where η is a unitless factor known as the pile flexibility factor calculated as

$$\eta = \left(\frac{L}{D}\right)\left(\frac{A_p}{A}\right)\left(\frac{G}{E_p}\right) \tag{6}$$

where D is the pile diameter, A_p is the lateral area of the pile, and G is the soil small strain shear stiffness at a reference pressure equal to the vertical effective stress at the pile tip. According to Said et al. (2009), τ_{res} is calculated assuming vertical force equilibrium using

$$\tau_{res} = \frac{A\, q_{p-res} - W}{A_p} \tag{7}$$

where W is the pile weight.

Since the centerpiece of the MEN approach (Eq. 1) has been derived for sandy soils, it is subject to question whether the MEN approach can be used for other ground conditions, such as that of the BEST where the soils is predominantly comprised of loose to medium dense silty sand. Noting that q_c is relatively low in such soils compared to sand with low fines content, the increase in radial stresses due to the pile installation process may not be properly predicted using the MEN approach.

3.4.2. Cavity Expansion (CE) approach

The second approach studied herein for numerical simulation of FDP is known as Cavity Expansion (CE) and was introduced by Krasiński (2014). CE approach is simulated using an updated mesh option and consists of five phases, schematically shown in Fig. 7(b). Once geo-static stresses are applied to the model following the K_0-procedure, a cavity is simulated by removing the soil volume with an initial radius (r_0) smaller than that of the pile ($r = D/2$). To take into account the radial displacements induced in the soil by the displacement tool, the primary cavity is expanded by applying a displacement boundary condition of $\Delta r = r - r_0$, resulting in a secondary cavity with a radius of $r = D/2$. To avoid unrealistic stress concentrations close to the head and tip of the pile, the expansion is gradually decreased to zero within the top and bottom 0.5 m of the pile. Simultaneously, concrete properties are assigned to the unpushed triangular masses t_1 and t_2 [Fig. 7(b)] to resemble the cylindrical pile geometry. An important assumption within this modeling phase is the adoption of a proper r_0, the value of which is indicated to be obtained from a number of trial analyses. However, in accordance with Krasiński (2014) and given the comparability of dimensions of the piles in this study (L = 9.5 m, r = 0.225 and 0.15 m) with the one simulated and reported in the former (L = 8.85 m, r = 0.18 m), r_0 is selected as $r/2 = D/4$.

In the third phase and to account for auger penetration-induced stresses around the installation zone, a high pressure, q_{cb}, is assigned to the base while hydrostatic pressure due to placement of fresh concrete is applied to the shaft wall. In a subsequent phase, the auger is withdrawn, and hydrostatic concrete pressure is applied to the excavation base as well. To model the pile, the removed soil volume is activated again during the fifth phase, to which hardened concrete properties are assigned, while interface elements are introduced between the pile and surrounding soil. Finally, a static head-down loading test is performed.

It is noted by Krasiński (2014) that by applying a base pressure larger than the hydrostatic pressure, the soil below the pile will be preloaded, which leads to a stiffer response during the pile loading. In CE approach, prediction of the pile load-movement behavior requires calibration of the preloading pressure q_{cb} based on pile load tests in a specific site. As this calibration was not possible at the BEST, the value suggested by Krasiński (2014) (q_{cb} = 1800 kN/m^2) was adopted in the present study as the pile geometries of the two studies being comparable. Moreover, Krasiński (2014) assumed a zone with approximately 10% reduced shear strength around the pile to mimic the pile soil contact. In this study, such a reduction in shear strength was directly applied to the intermediate interface at the pile-soil contact ($\delta / \phi' = 0.9$, where δ is the interface friction angle). For the sake of consistency, the same reduction has been applied to the interfaces for all FDP simulation approaches (MEN, CE, CE-SL and CE-VS).

3.4.3. Cavity Expansion with Sub-Layering (CE-SL) approach

Unlike the MEN and CE approaches, in the Cavity Expansion with Sub-Layering (CE-SL), the geometry of the tool used to drill the pile hole is attempted to be taken into account. As shown in Fig. 8, the FDP drilling tool consists of two auger segments mounted at the top and bottom of the displacement body, and a sacrificial boring tip fitted to its base, the geometry of all which may vary for different projects. However, a unique installation procedure is followed, which includes loosening (lower auger), densification and stabilization (displacement body), and post-densification during extraction (upper auger). The most important feature of an FDP tool that affects stresses and deformations around the pile is diameter which varies for different segments, the drilling blade (D_1), the drilling string below the displacement body (D_2), the displacement body (D_3), and the drilling string above the displacement body (D_4).

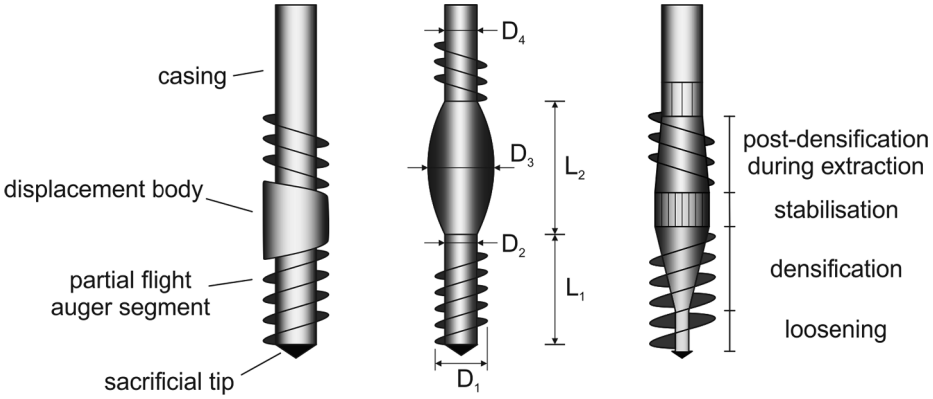

Fig. 8. Drilling tool details.

In the CE-SL approach, the pile installation process and the subsequent head-down loading test are performed in separate numerical models [Fig. 7(c)]. In the first model, the first two phases discussed in the CE approach are carried out, and the increased lateral stresses, σ'_h, over depth are used to obtain an updated K_0 profile which is due to the advancement of the FDP drilling tool. The changes in σ'_h are considered within a zone of $2D$ around the pile. Assuming that the soil densification and corresponding changes in lateral stresses are mainly induced by the displacement body, the radial displacement applied to the model [Fig. 7(c)], Δr, can be calculated as $\Delta r = 0.5(D_3 - D_2)$, and the initial hole radius is therefore obtained as $r_0 = r - \Delta r$. Dimensions of the FDP drilling tools used at the BEST were $D_3 =$ 450 mm and $D_2 =$ 350 mm for the pile C2, and $D_3 =$ 300 mm and $D_2 =$ 220 mm for the pile E1. In this approach as well, unpushed triangles of 0.5 m height at the top and bottom of the initial hole are considered to avoid numerical instabilities as smooth transitions are allowed between the elements which undergo large displacements and those that undergo smaller or zero displacements. Unlike the CE approach, the hydrostatic pressure of the liquid concrete has not been taken into account.

In the second (sub-layering) model, sub-layers of 1 m thickness are assigned to the model with an average K_0 value obtained from the first model being applied to each. Afterward, the final pile geometry is simulated following the wished-in-place technique, similar to the final stages of the previously discussed methods before carrying out the head-down loading test.

3.4.4. Cavity Expansion with Vertical Shearing (CE-VS) approach

The last FDP modeling approach investigated in this research is based on the concept proposed by Basu et al. (2013) for capturing installation effects of drilled displacement (DD) piles. In their approach, the pile installation process is simulated in three phases: (1) cavity expansion considering the radial displacement in the soil due to advancement of the drilling tool, (2) torsional shearing combined with vertical shearing as the drilling tool moves downward and (3) vertical shearing as the drilling tool moves upward. By conducting a series of FEM simulations, Basu et al. (2013) derived equations to estimate the ratio between the pre- and post-densification lateral earth pressure coefficients for DD piles in sandy soils. As the BEST is mainly comprised of silty sands and clays, those equations are not necessarily resulting in a good prediction. For this reason, the general concept of the FEM analyses performed by Basu et al. (2013) is transferred to simulate the FDP installation process for the BEST.

It has to be noted that Basu et al. (2013) performed one-dimensional FEM analysis using 8-node elements with an additional out-of-plane Degree of Freedom (DoF). However, as the 2D axisymmetric platform used in this study does not incorporate an out-of-plane DoF for application of the torsional shearing, an alternative series of phases are employed herein to mimic the CE-VS approach. After initiation of geostatic stresses according to the K_0-approach, the following sequence of simulation phases are pursued [Fig. 7(d)]: (1) deactivation of the excavated soil volume of r_0 radius, (2) cavity expansion by applying a displacement boundary condition of Δr, (3) vertical shearing to account for the downward movement of the displacement tool, (4) vertical upward shearing to simulate the extraction of the drilling tool, and (5) activation of the pile volume elements and assignment of concrete material as well as activation of interfaces elements. Finally, a static head-down loading test is performed using the approach discussed in previous sections.

It has to be noted that in contrast to Basu et al. (2013), the radial displacement for cavity expansion in phase 2 has been determined from drilling tool geometry similar to CE-SL. The vertical shearing in phases 3 and 4, however, follow the concept proposed by Basu et al. (2013), where downward and upward displacement boundary conditions are applied to the shaft wall until the changes in normal and shear stresses at all points in the surrounding soil become negligible and further displacement does not affect the stresses. It is worth mentioning that similar to the previously discussed approaches for FDP modeling, the friction angle of interface elements are reduced to 90% of the mobilized friction in the surrounding soil.

3.5. Modeling approach for numerical simulation of Expander Body

In cases where the shaft friction provides insufficient bearing capacity for a pile to carry high service loads, the Expander Body (EB) has been found to be very practical and has been used for decades (Massarsch and Wetterling, 1993; Terceros et al., 1995). Attached to the pile toe, an EB consists of a folded steel tube which can be inflated by injection of cementitious grout. Thus, by increasing the toe area, the EB enhances the base resistance of the pile significantly. Recent advancements in EB construction systems also enable pressure grouting below the EB, referred to as post grouting, to assure full contact between the EB and the soil (Terceros and Massarsch, 2014) and to provide preloading of the soil below the EB. The post grouting pressure depends on the soil type, density, and the depth of EB installation and has been reported by Terceros and Massarsch (2014) to vary between 1.4 to 3.1 MPa.

Although the EB inflation varies the physical properties of the soil in its surrounding (i.e. density, porosity), variation of the stress field and exchange of the soil condition from at-rest to passive state have the most dominant impact on the pile bearing capacity. This can be attributed to higher coefficient of lateral earth pressure as well as full mobilization of shear resistance in the surrounding soil of EB. In the present study, the evolution of the stress field and lateral earth pressure around the EB have been addressed by applying radial deformation around the EB in the numerical simulations while the physical impacts have been neglected. In this frame, it is assumed that the auger drilled cavity for the EB to be placed into is about 0.3 m, corresponding to the diameter of the displacement tool used for the installation of the pile E1. In the numerical model, soil elements of this excavated zone are first deactivated [Fig. 9 (a)]. Afterward, the cavity expansion due to the inflation of the EB is modeled following the procedure described previously for the CE approach in FDP simulation [Fig. 9 (b)]. Knowing

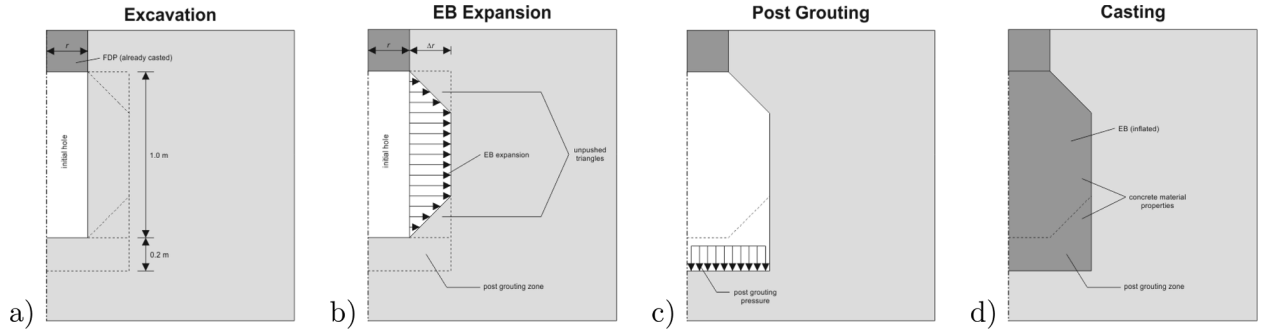

Fig. 9. Numerical simulation stages of the EB installation and inflation process.

that $D_3 = 0.41$ m (EB diameter after expansion), Δr can be calculated as $\Delta r = 0.5(D_3 - D_2) = 0.5(0.41 - 0.3) = 0.055$ m.

It has to be noted that the initial length of the EB was measured to be 1.2 m. However, a proper installation of EB with a uniform expansion (as measured by the EB inflation in air) demands a 20 cm length shortening. Since no unusual observation was reported during the EB installation at the BEST, such a length reduction was considered as a certain kinematic condition in this research. The post grouting procedure can be separately simulated by first deactivating the 0.2 m thick zone at the bottom of the simulated EB, and then applying the post grouting pressure at the base as shown in Fig. 9 (c). Since post grouting pressure was not reported at the BEST, trial analyses carried out at the preliminary stage of the study indicated a very marginal influence of the post grouting pressure (i.e., 1–3 MPa) on the pile load-movement curve. Therefore, a typical value of 2.5 MPa has been adopted as a deterministic value in the numerical simulations. Finally, elements within the excavated zone are activated, and hardened concrete properties are assigned, and interface elements with an interface friction angle of $\delta = \phi$ (i.e. $R_{\text{int}} = 1.0$) are introduced at the boundary of the simulated EB installation zone [Fig. 9 (d)].

4. Results and discussion

4.1. Bored pile

For the sake of completeness of this project, the results of the numerical simulation of the static head down load test of bored pile A3 are briefly summarized in this section. In a preliminary study, the field measurements from BEST have been compared to the numerical simulation using the optimistic, average and conservative parameter sets in terms of the load-movement curve [Fig. 10 (a)] and the load distribution over the depth (length of the pile) at 30 mm head movement [Fig. 10 (b)].

As can be seen from Fig. 10 (a) the constitutive parameters significantly influence the load-movement prediction. Furthermore, a very good agreement with the field measurements could be obtained by applying the average parameter set. However, a comparison of the load distribution over the depth [Fig. 10 (b)] revealed that by following the average parameter set, the numerical simulation slightly underestimates the pile load between depths of 2–5 m. This is likely because the numerical model has overestimated the shaft interface resistance, and in turn, the load transferred from the pile to the surrounding soil, in layer L1. Therefore, the remaining pile load to be transferred to the soil below the depth of 2 m has been slightly underestimated. Note that here, the shaft interface resistance has been assumed to be proportional to the soil shear strength. - Further improvement can be achieved by parameter optimization, which will be conducted in Section 5.3.

4.2. Full-displacement pile

The four methods of numerical modeling of FDP presented in Section 3.4 are investigated in this section using the load-movement and load distribution responses obtained from the static head-down loading test on the pile C2 from the BEST. Similar to the bored pile, the optimistic, average, and conservative parameter sets have been used to provide a better comparison. The load-movement curve and the load distribution over the depth of installation at 43.5 mm head movement have been presented for the pile C2 in Figs. 11 and Figs. 12, respectively.

It can be seen in Fig. 11(a) that the MEN approach mainly under predicts the load-movement behavior of FDP piles in conjunction with the average and conservative material parameter sets. Although the optimistic estimates from the MEN method provide a reasonable match, adopting such an approach for the selection of soil parameters seems to lack a fair justification from an engineering point of view. Looking at the results obtained from all sets of material parameters, one concludes that compared to other investigated modeling approaches, the MEN approach predicts a significantly softer load-movement behavior for the pile C2. The resulting poor predictions using the average parameter set reveal the irrelevance of this method for this specific site, and highlight the inadequacy of the MEN approach for non-sandy soils.

Considering the results of the CE, CE-SL and CE-VS approaches presented in Fig. 11(b)- to Fig. 11(d), it is apparent that the best match between the field measurements and the simulations is obtained by using the average material parameter set. In addition, the results of these three approaches deviate only over a small range. This holds for the conservative, average, and optimistic material parameter sets. For instance, the standard deviations at 43 mm movement are obtained as 12%, 5% and 1%, respectively for CE, CE-SL, and CE-VS approaches. Evaluating the movements of the piles under service load conditions with movements < 25 mm, CE-SL method resulted in the best agreement with the measurements, while CE method slightly underpredicts and CE-VS overestimates the pile resistance. However, a clearer distinction can be made between those three approaches by comparing the load distribution responses.

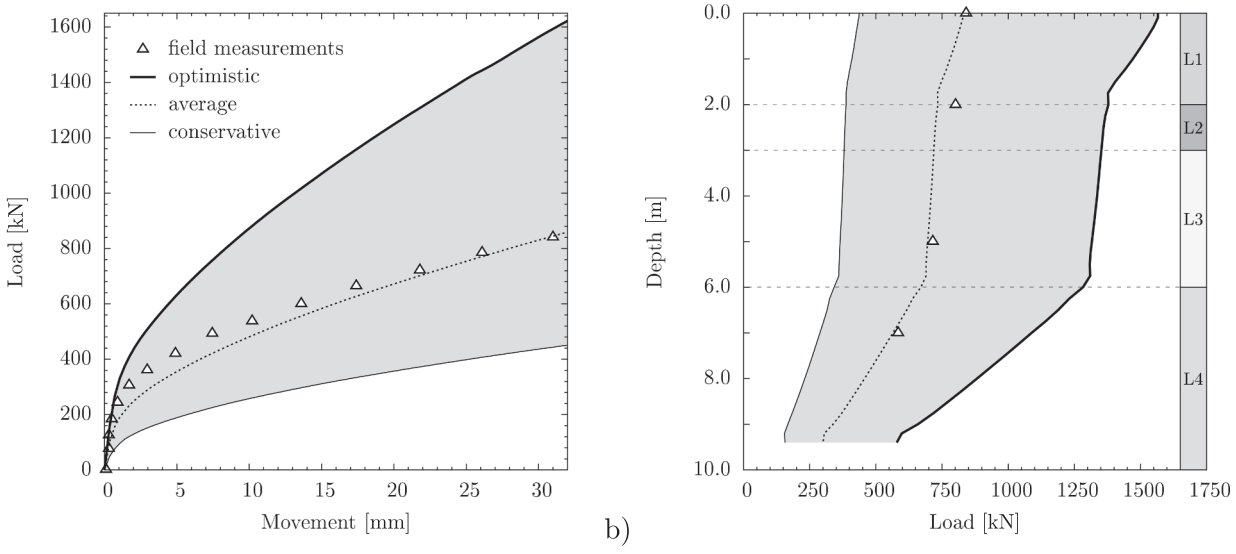

Fig. 10. Load test of a bored pile: Comparison of (a) the load-movement curves and (b) the load distribution over depth at 30 mm head movement using the optimistic, average and conservative material parameter sets.

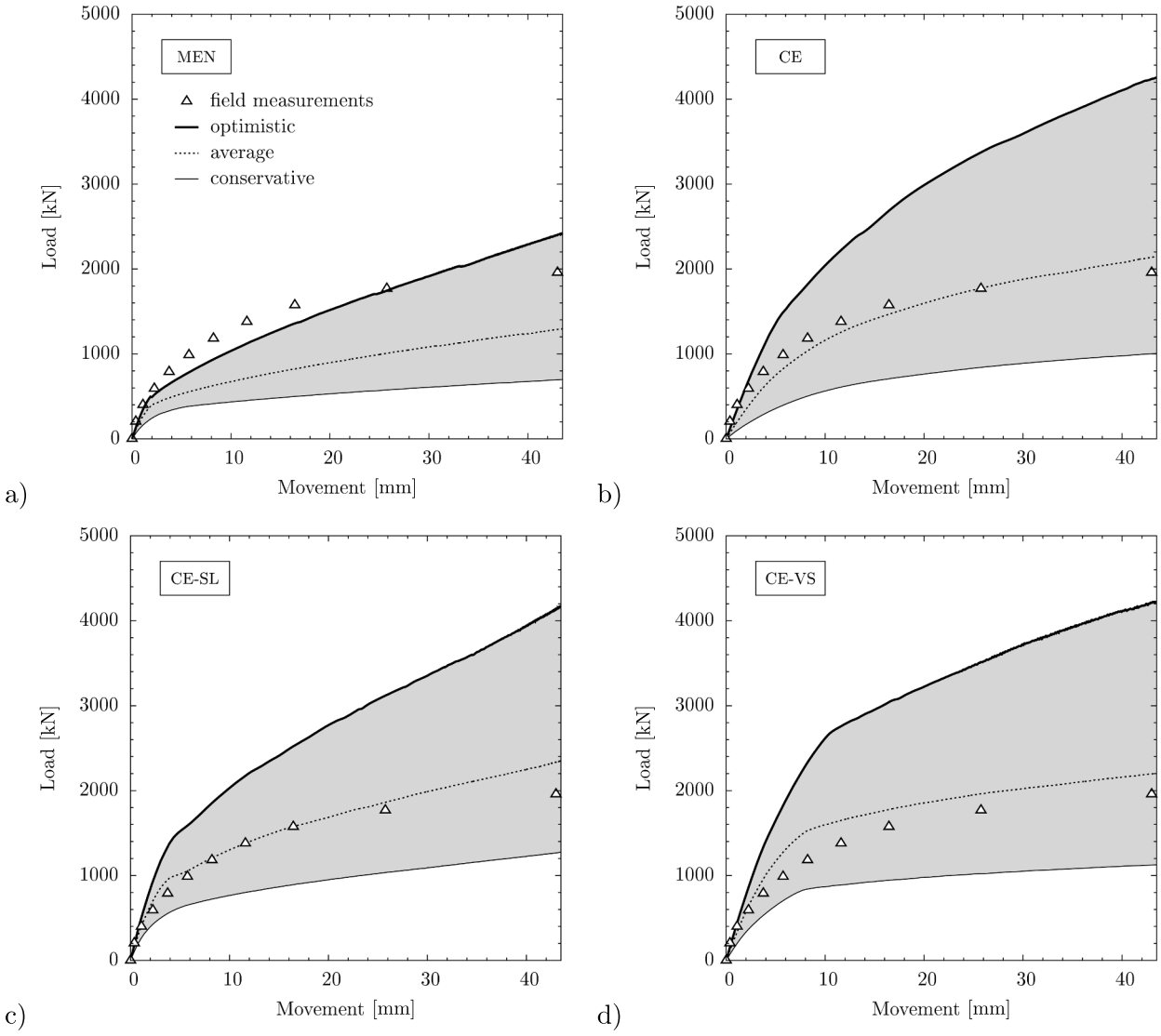

Fig. 11. Load test of a full-displacement pile: Comparison of load-movement curves for (a) mixed empirical numerical approach (MEN), (b) cavity expansion (CE) approach, (c) cavity expansion approach with sub layering (CE-SL) and (d) cavity expansion approach considering vertical shearing (CE-VS) using the optimistic, average and conservative material parameter sets.

It can be observed from Fig. 12(a) that the distribution of loads at various depths are underestimated in the MEN approach by using the average material parameter set. Only the load at 7.5 m depth matches the field measurements indicating that the shaft resistance within all layers has not been mobilized sufficiently. Due to the absence of load measurements below 7.5 m depth, precise assessment of the pile tip resistance in any of these methods is not within the scope of this comparison. In Fig. 12(b) the load distribution measurements are compared with CE approach. Although the average parameter leads to a good match with the measurements, it was not possible to obtain a smooth monotonous curve, similar to those obtained from other methods. It should be noted that results for CE approach presented herein are hence smoothened by averaging five consecutive values over depth. This procedure in the CE approach was inevitable as the strains in the symmetric axis increased significantly in the simulation phase, where the initial cavity was radially expanded. A possible reason for this observation may be the updated mesh option which led to distorted elements with aspect ratios larger than 8. In contrast to the MEN and CE approaches, the CE-SL and CE-VS approaches presented in Fig. 12(c) and Fig. 12(d), respectively, are relatively comparable to the field measurements when using the average material parameter set. Still, it has to be noted that both approaches lead to a slight overestimation of the load distribution over the entire length of the pile. An explanation of this overestimation can be given by analyzing the load transfer between the pile and the surrounding soil within each layer separately. Compared to the field measurements, it is found that the shaft resistance has been overestimated in the numerical simulation for layers L1 and L4, which is indicated by a larger increase in the load transfer. Furthermore, the comparison revealed that the shaft resistance of layers L2 and L3 has been underestimated in the numerical simulation as shown by an almost constant load transfer within these layers. However, as the contribution of layers L2 and L3 is small compared to the contribution of layer L1 and L4, the overall prediction of the load distribution has been overestimated. Nevertheless, it has been shown that both CE-SL and CE-VS approach are in better agreement with the measurements of pile C2 than MEN and CE approach. CE-SL and CE-VS approach will, therefore, be further investigated in the following section for numerical simulation of the FDP with an attached expander body (pile E1).

4.3. Full-displacement pile with attached expander body

To investigate different EB modeling scenarios for pile E1, CE-SL and CE-VS approaches (Section 3.4) have been selected for FDP simulation followed by the inflation and post grouting procedures (Section

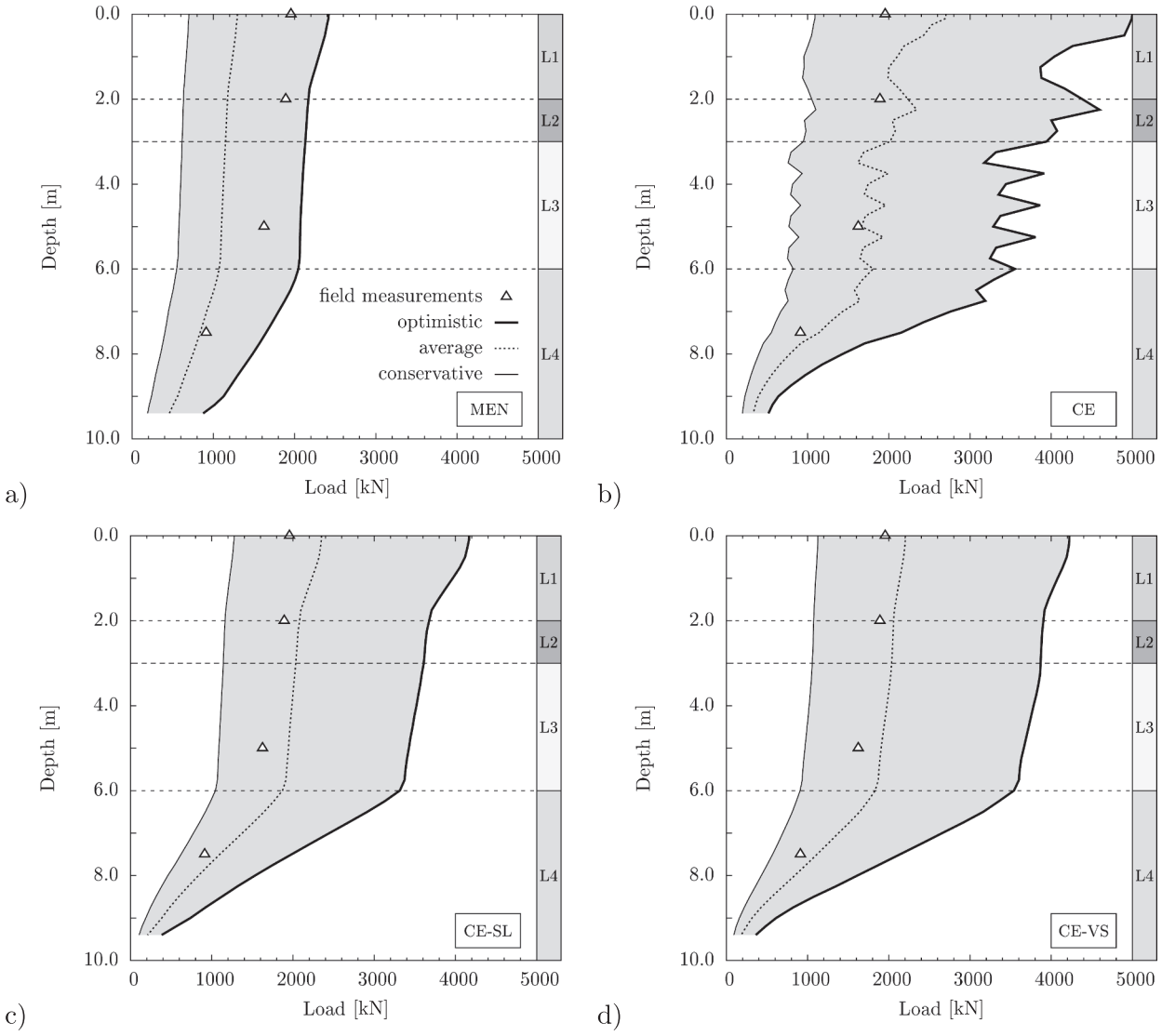

Fig. 12. Load test of a full-displacement pile: Comparison of load distribution over depth at 43.5 mm head movement for (a) mixed empirical numerical approach (MEN), (b) cavity expansion (CE) approach, (c) cavity expansion approach with sub layering (CE-SL) and (d) cavity expansion approach considering vertical shearing (CE-VS) using the optimistic, average and conservative material parameter sets.

3.5), resulting in four different simulation setups. Additional two simulations are performed using both EB inflation and post grouting procedures for each of the FDP modeling approaches. Similar to Sections 4.1 and 4.2, the influence of input parameters is studied by evaluating the simulation results for the conservative, average, and optimistic estimates. The radial displacement applied in CE-VS and CE-SL approach has directly been determined from the drilling tool geometry used to install pile E1 as $\Delta u = 0.5(D_3 - D_2) = 0.5(300\,\text{mm} - 220\,\text{mm}) = 40\,\text{mm}$. The results are presented in Fig. 13 in terms of the load-movement curve (left) and load distribution over depth at 25 mm head movement (right). However, since field measurements were not provided to obtain the load distribution, only the results of the numerical simulation are presented here.

As shown in Fig. 13, CE-SL approach (blue curves) initially predicts softer pile load behavior compared to CE-VS approach (black curves). This observation holds for post grouting (PG) in Fig. 13(a), EB inflation (INF) in Fig. 13(c), and combination of both procedures (PG + INF) in Fig. 13(f), for the conservative, average, and optimistic material parameter sets. Comparing the field measurements against numerical results, it appears that regardless of the modeling approach, the load-movement curve of pile E1 has been overestimated by using the average parameter set. Although the difference between the results of numerical simulations and field measurements decreases at larger head movements, the overall quality of the predictions is not satisfactory. However, it has to be noted that in contrast to the load-movement curve for the bored pile (A3) and full-displacement pile (C2), measurements in Figs. 13(a,c,e) do not follow the general hyperbolic trend but rather a linear one. Such linear load-movement behavior in field measurements may be due to a lack of full initial contact between the pile tip and the soil below, resulted from the inflation of EB which may have now been fully recovered by post grouting. Therefore, it is subject to question whether the observed differences should be attributed to the approximation of soil properties, the numerical modeling approach, or some potential issues arisen during FDP and EB casting and loading in the field. The comparison of the pile head loads at 50% and 100% pile head movements for different parameter sets has been presented in Table 3 for various types of piles. As seen, at 50% pile head movement, employing the conservative parameters in the numerical simulations leads to approximately 35–50% reduction in the pile head load compared with the value obtained by adopting the average parameters; using the optimistic parameters increases the pile head load in a range of

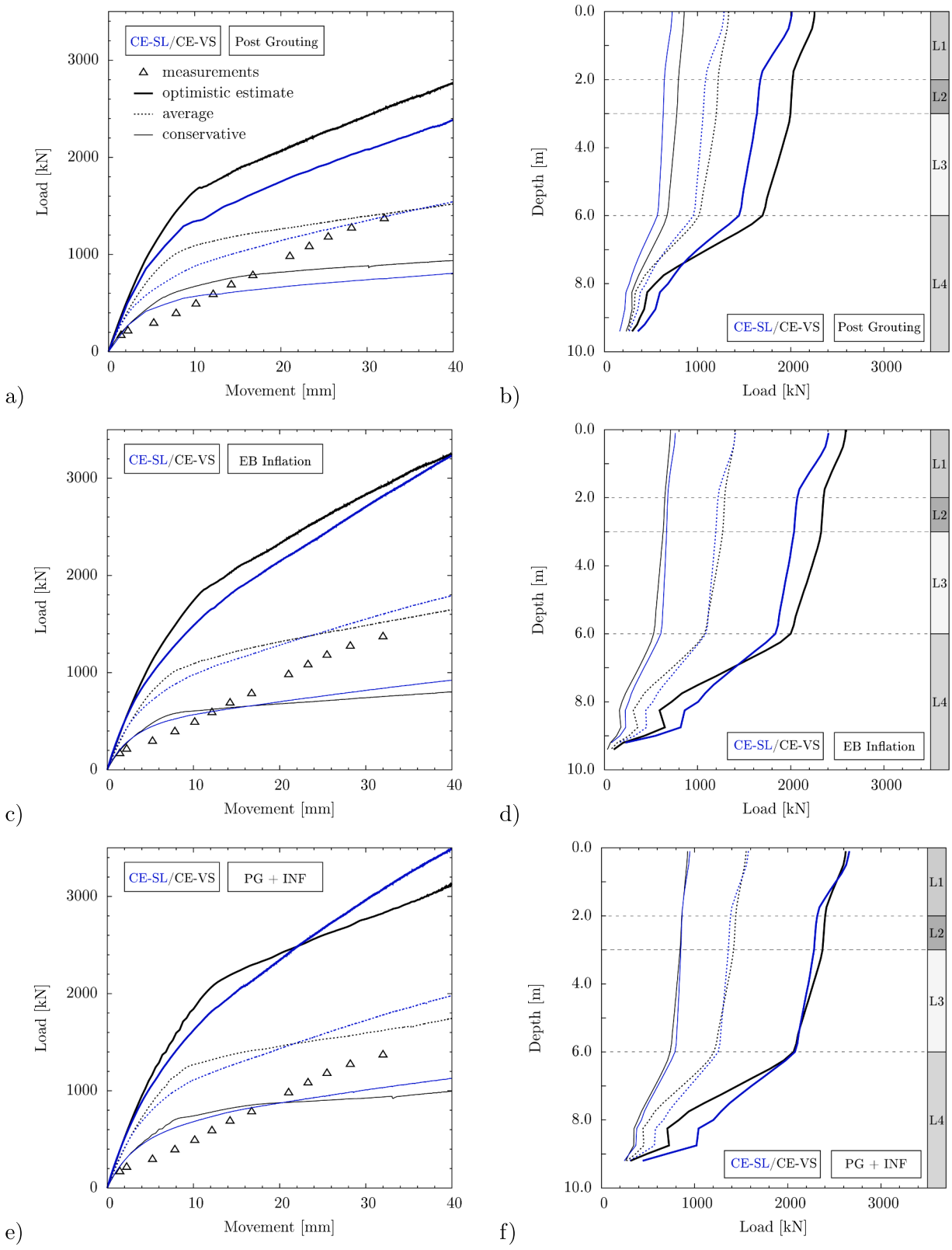

Fig. 13. Load test of a full-displacement pile with attached expander body: Comparison of (left) load-movement curve and (right) load distribution over depth at 25 mm head movement for CE-VS and CE-SL in combination with (a,b) EB post grouting (PG), (c,d) EB inflation (INF) and (e,f) EB post grouting and inflation (PG + INF) using the optimistic, average and conservative material parameter sets.

approximately 55–85%. At 100% of pile head movement, the influence of the parameters is slightly greater (i.e., 40–55% for the conservative and 55–100% for the optimistic parameter sets).

5. Parametric study

Previous studies have revealed that uncertainty in the constitutive parameters can be directly propagated into the numerical predictions.

Table 3
Influence of the parameter sets (average, conservative, optimistic) and the modeling approach on the pile head load obtained for the bored pile, the full-displacement pile, and the full-displacement with expander body at 50% and 100% pile head movement.

Pile type	Modeling approach		Pile head load (at 50% head movement)			Pile head load (at 100% head movement)		
	FDP	EB	avg. [kN]	cons.	optimis.	avg. [kN]	cons.	optimis.
Bored pile	–	–	600	−47% (16 mm)	+84%	860	−48% (32 mm)	+89%
FDP	MEN	–	930	−42%	+71%	1300	−46%	+87%
	CE		1660	−52%	+88%	2150	−53%	+98%
	CE-SL		1750	−44%	+64%	2350	−46%	+77%
	CE-VS		1890	−47% (21.75 mm)	+76%	2200	−49% (43.5 mm)	+92%
FDP + EB		PG	1180	−42%	+54%	1610	−48%	+56%
	CE-SL	INF	1280	−46%	+67%	1790	−49%	+80%
		PG, INF	1430	−39%	+64%	1980	−43%	+76%
		PG	1260	−35%	+63%	1520	−38%	+81%
	CE-VS	INF	1320	−48%	+77%	1640	−51%	+98%
		PG, INF	1460	−40% (20 mm)	+65%	1750	−43% (40 mm)	+79%

MEN: Mixed Empirical-Numerical approach, CE: Cavity Expansion approach, CE-SL: Cavity Expansion with Sub-Layering approach, CE-VS: Cavity Expansion with Vertical Shearing approach.
PG: post grouting, INF: EB inflation.

In a preliminary study, conservative, average, and optimistic estimates for more than 50 individual constitutive parameters have been suggested with reference to the in situ measurements and using the empirical correlations to HSS model parameters. However, a more detailed investigation is necessary to better understand the influence of individual input parameters on the outputs of the numerical model. For this reason, sensitivity analyses can be used to identify soil parameters with significant influence on the model output. In geotechnical engineering, sensitivity analysis has been widely used by several researchers for various problems. In general, there are two approaches for sensitivity analysis, namely Local Sensitivity Analysis (LSA) and Global Sensitivity Analysis (GSA).

In LSA, the derivatives of the inputs are calculated by variation of the input parameter space with the restriction that inputs are only varied independently of each other. In this way, the computational effort is kept comparatively small, but the gain in information is limited. However, LSA is only valid for small variations in the input space or models showing linear behavior. Further shortcomings of LSA have also been shown by Zhao et al. (2018). Since correlation effects between input parameters cannot be evaluated with LSA due to individual variation of parameters, it is recommended to analyze parameter sensitivities via GSA. In GSA, all input parameters are varied at the same time to quantify the impact of the input variances on the output variances with respect to possible correlation effects. Still, since the number of unknown soil parameters is very large, LSA is used to significantly decrease this number of parameters, which will be further investigated in GSA.

5.1. Local sensitivity analysis

In this study, LSA is performed to indicate the influence of the input parameters x_j, on the model outputs (i.e., pile loads for different head movements) y_i, using a scaled sensitivity (SS) index. To determine the scaled sensitivity index $SS_{i,j}$, the changes in the model outputs due to variation of the input parameters are analyzed. To be more specific, the derivatives of each model output are numerically approximated according to Eq. (8).

$$SS_{i,j} = \left(\frac{\partial y_i}{\partial x_j}\right) x_j \approx \left(\frac{\Delta y_i}{\Delta x_j}\right) x_j = \left[\frac{y_i(x_j + \Delta x_j) - y_i(x_j)}{\Delta x_j}\right] x_j \tag{8}$$

where y_i, x_j, and Δx_j state the model output, model parameters (e.g., average friction angle of layer L1) and the variation of the model parameter, respectively. The average of the $SS_{i,j}$ values gives an overall sensitivity of y_i to the model parameter x_j and can be described by the composite scaled sensitivity CSS_j according to Eqn. 9.

$$CSS_j = \sqrt{\frac{1}{N}\sum_{i=1}^{N} SS_{i,j}^2} \tag{9}$$

To enable quantitative comparison of CSS values associated with different parameters, scaled sensitivity measure γ_j is used, which scales all CSS values to [0,1].

$$\gamma_j = \frac{CSS_j}{\max(CSS)} \tag{10}$$

In this study, the following material parameters of layers L1 - L4 have been varied within an LSA frame to determine the individual influence on the output, namely pile head load: ϕ', ψ, E_{50}^{ref}, E_{oed}^{ref}, E_{ur}^{ref}, G_0^{ref}, $\gamma_{0.7}$, m and K_0. Though, to avoid misinterpretation of the sensitivity towards specific parameters, the empirical relations between E_{50}^{ref}, E_{oed}^{ref} and E_{ur}^{ref} are not used in this part. Therefore, all parameters are considered to be independent. However, since only small variations can be applied in LSA, a deviation of ± 5% has been assumed for all input parameters and scaled sensitivities have been evaluated for pile head loads at 30% and 100% of the final pile head movement, respectively. These loads have been chosen in order to analyze both the load-movement behavior at small and larger strains.

The results of the scaled sensitivity analysis are given in Fig. 14 in terms of the scaled sensitivity measure γ_j. To highlight the section of high sensitivity, a line pattern is added to the zone where the sensitivity of the parameters is larger than 0.01. Parameters with dominant influence on the model output can be identified as bars which intersect with the patterned area, for instance E_{50}^{ref} of layer L1 in Fig. 14(a), or ϕ' of layer L4 in Fig. 14(b). Combining the results for pile head loads at 30% and 100% of the final pile head movement including $E_{50,1}^{ref}$ and $K_{0,3}$ with $\gamma_j \approx 0.01$, a total number of 12 dominant parameters can be identified. Here, the additional index of the input parameters refers to the layer (L1-L4) to which they belong. However it should be noted that E_{50}^{ref}, E_{oed}^{ref} and E_{ur}^{ref} will not be treated as independent parameters in GSA. Otherwise, due to large ranges between lower and upper bound values, the ratios between these reference stiffnesses may change significantly, which is not consistent with engineering experience. Therefore, the ratios between E_{50}^{ref}, E_{oed}^{ref} and E_{ur}^{ref} will be kept constant and only E_{oed}^{ref} will be considered as independent parameter. Still, it should be emphasized that these ratios are dependent on the soil type and are not the same for each layer (e.g. Table 2). Hence, in GSA these 11 independent constitutive parameters will be further analyzed: ϕ' in L1, L3 and L4, ψ in L4, E_{oed}^{ref} in L1 and L4, G_0^{ref} in L4, $\gamma_{0.7}$ in L4, m in L4 and K_0 in L3 and L4 using the ranges given in Table 2.

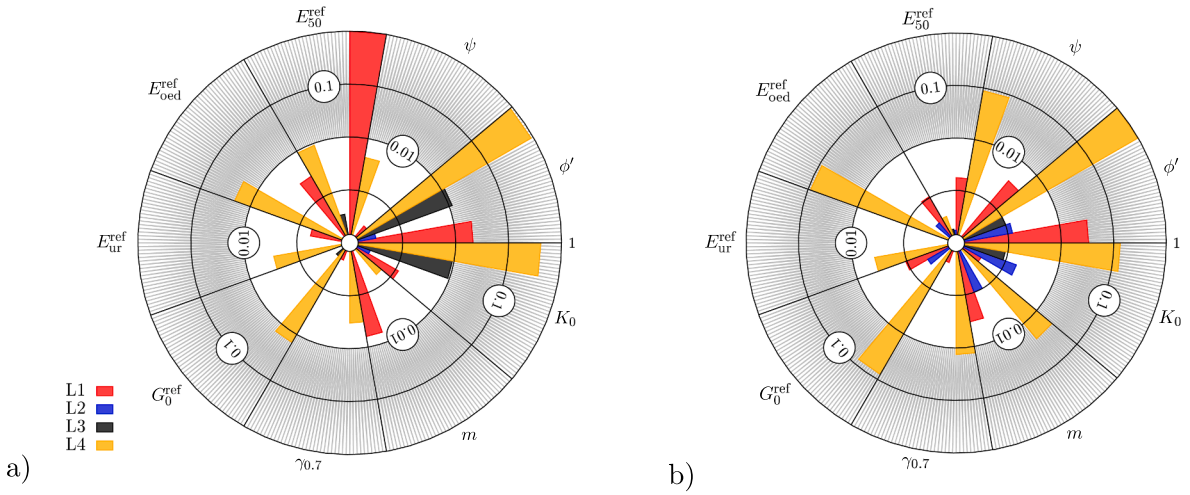

Fig. 14. Composite scaled sensitivity measure γ_j evaluated for loads at 30% (a) and 100% (b) pile head movement.

5.2. Global sensitivity analysis

Due to the fact that the pile load-movement responses include nonlinear behavior, the model output may vary in a wide range. Additionally, with reference to the possible correlation between multitudes of model inputs, the above-mentioned LSA is no longer applicable to closer rank the importance of the dominant parameters in the model. For this reason, GSA has to be carried out to assure that the results which have been obtained from LSA can be confirmed within smaller steps of pile head movement (i.e. $u_{20\%,40\%,60\%,80\%,100\%}$). To do that, a variance-based method of GSA is applied in this study, which was first introduced by Sobol (1993) and further developed by Saltelli et al. (2008). Previous studies have shown that the GSA analysis in accordance with variance-based method leads to promising results for geotechnical problems (Zhao et al., 2015; Zhao et al., 2018). Using this method, the impact of the input variances on the output variances can be quantified, taking into account the uncertainty contribution of a specific parameter as well as the correlated variations of other parameters. The total effect index S_{Ti}, which considers correlation effects, is determined according to Eqn. (11).

$$S_{Ti} = \frac{(\boldsymbol{y}_B - \boldsymbol{y}_{C_i})^T(\boldsymbol{y}_B - \boldsymbol{y}_{C_i})}{\boldsymbol{y}_B^T\boldsymbol{y}_B - 2n(\bar{\boldsymbol{y}}_B)^2} \tag{11}$$

Here $\boldsymbol{y}_A$, $\boldsymbol{y}_B$ and $\boldsymbol{y}_{C_i}$ are vectors containing model outputs (e.g. pile loads at predefined head movements) for matrices A, B and C_i, which are of dimension (n, s) and include random sets of parameters, with n being the number of samples generated and s the number of inputs (here $s = 11$ according to LSA results). Matrix C_i contains the same array as B, but the ith column has been replaced by the ith column of matrix A. $\bar{\boldsymbol{y}}_A$ and $\bar{\boldsymbol{y}}_B$ are the mean values evaluated from components of $\boldsymbol{y}_A$ and $\boldsymbol{y}_B$.

To apply GSA, a large number of different input combinations has to be evaluated in order to have a proper distribution of parameter sets in the s-dimensional space. In the present study, well distributed near-random sample points in the entire s-dimensional input space are generated according to statistical Latin Hypercube Sampling (LHS) procedure (McKay et al., 1979). Since quantifying this number is highly dependent on the model complexity as well as the constitutive model employed, the necessary evaluations may vary up to 10,000 or more (Saltelli et al., 2008). To overcome the disadvantage of high computational costs which arises from the large number of evaluations necessary (compared to LSA) as well as from the calculation time of each simulation itself, a meta- or surrogate model providing appropriate responses for predefined observation points will be used to replace the finite element simulation model. In this study POD-ERBF, i.e. Proper Orthogonal Decomposition combined with Extended Radial Basis Function (Müller and Messac, 2005; Khaledi et al., 2014), which is an extension of POD-RBF (Buljak, 2011), is used to build up the meta-model. For this purpose 500 samples of input combinations in the s-dimensional space have been created using LHS technique and pile loads at different pile head movements have been computed using the finite element model. After the creation of the meta-model from these input combination and corresponding outputs, another 100 validation points are generated via LHS method to evaluate the accuracy of the constructed meta-model. To this end, the standard error measure is investigated: $R^2 = 0.95$. Since evaluations of the output responses using the meta-model approach can be carried out within seconds, also GSA can be conducted with an acceptable computational cost.

The ranges used in GSA may, in general, be defined in different ways: (1) assuming a deviation of inputs chosen, as proposed for the scaled sensitivity analysis performed in Section 5.1, (2) applying typical parameter ranges on the basis of engineering judgment, mostly applied to synthetic problems, (3) referring to statistical analysis of in situ data. In this study, the latter one is chosen as the input parameter ranges used are based on a statistical analysis of the in situ tests performed at BEST. Therefore, the parameters in GSA are assumed to vary between the conservative and optimistic estimate given in Table 2.

The results of the GSA are presented in Fig. 15 in terms of total sensitivity index S_{Ti}. From the data in Fig. 15, it is apparent that constitutive parameters of layers L1 and L3 have negligible influence on pile head load. Similar to the results of LSA, parameters of layer L4 are the most important ones with respect to their influence on the pile head load. However, by focusing only on the final pile head load ($u_{100\%}$), we can distinguish between two groups of key parameters within this layer: ϕ_4', $E_{oed,4}^{ref}$ and $K_{0,4}$ with major influence ($S_{Ti} > 0.2$) and ψ_4, $G_{0,4}^{ref}$, $\gamma_{0.7,4}$ and m_4 with medium influence ($S_{Ti} < 0.1$). A comparison between LSA and GSA results reveals that there are some key parameters with more important influence on the model output among the 11 dominant parameters obtained via LSA. However, the over- and underestimation of the pile shaft resistance respectively in layers L1 and L3, as shown for instance in Fig. 10 (b), indicates the need for further investigation of the parameters of these layers. Accordingly, 11 dominant parameters which have been confirmed by GSA have been further studied in the parameter identification.

5.3. Parameter Identification via Inverse Analysis

Though choosing a proper method of simulation is essential for an adequate numerical model, material parameters have to be properly identified. The material parameters are often calibrated at the element

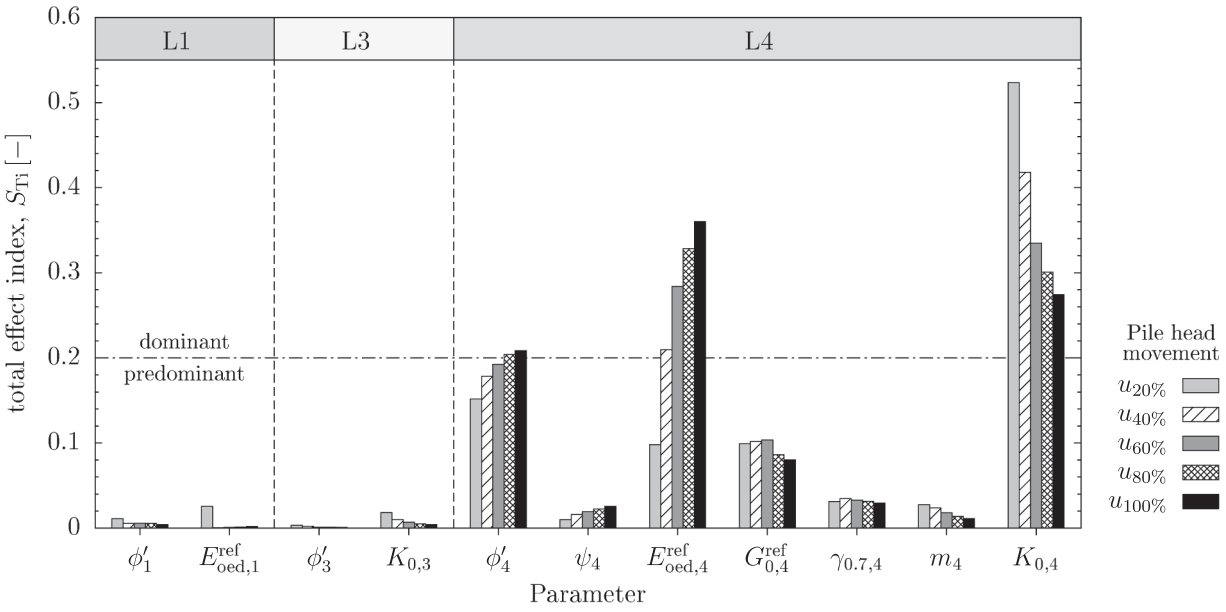

Fig. 15. Total effect index S_{Ti} for total loads at pile head movements up to 30 mm.

level based on laboratory and in situ tests, however the measurements obtained from field load tests or on-site monitoring can be used to fine tune the parameters and to bound their uncertainties. In the present study, the parameters of the HSS model are identified via an inverse analysis to find the optimum set between the measured load test data and the numerical simulation results. To compare and evaluate different parameter combinations, first, an objective function is defined according to Eqn. 12 as the sum of normalized differences between numerical simulation and measurement.

$$f(\boldsymbol{X}) = \frac{1}{M}\sum_{i=1}^{M}\left[w_i\left(\frac{y_i^{calc}(\boldsymbol{X}) - y_i^{meas}}{y_i^{meas}}\right)^2\right] \tag{12}$$

Here, $\boldsymbol{X}$ is the vector of HSS model parameters investigated in LSA and GSA which need to be identified, $y_i^{calc}(\boldsymbol{X})$ and y_i^{meas} are the calculated results and load test measurements, M is the number of measurements and w_i is an optional weighting factor which is assumed to be 1 in this study. To identify the parameter set which corresponds to the best fit between the load test and the numerical simulation, the aim of the inverse analysis is to minimize the objective function, since lower values of $f(\boldsymbol{X})$ indicate smaller differences at the observation points analyzed. This aim can be achieved by using Genetic Algorithms (GA) or Particle Swarm Optimization (PSO) (Clerc, 2013), the latter one being applied to solve the minimization problem in this study. The main operations performed in PSO algorithms are given in Eqs. (13) and (14) for velocity and position update, respectively.

$$V_k(t) = \underbrace{\eta V_k(t-1)}_{\text{momentum}} + \underbrace{c_1 r_1 (X_k^L - X_k(t-1))}_{\text{cognitive component}} + \underbrace{c_2 r_2 (X^G - X_k(t-1))}_{\text{social component}} \tag{13}$$

$$X_k(t) = X_k(t-1) + V_k(t) \tag{14}$$

The velocity $V_k(t)$ of a single particle k at time step t is influenced by three parts, namely the momentum, i.e. its velocity at previous time step $V_k(t-1)$, the cognitive component, i.e. its local best position X_k^L and the social component, i.e. the swarm's global best position X^G. The position $X_k(t)$ of a single particle k at time step t is then calculated by summation of the previous position $X_k(t-1)$ and the actual velocity $V_k(t)$. For further details regarding PSO the reader is referred to Clerc (2013). Since the optimization process with PSO requires a high number of calculations, the meta-model created for GSA in Section 5.2 is employed again to reduce computational costs.

In this study, inverse analysis has been used to calibrate the parameters investigated in LSA and GSA (ϕ'_1, $E^{ref}_{oed,1}$, ϕ'_3, $K_{0,3}$, ϕ'_4, ψ'_4, $E^{ref}_{oed,4}$, $G^{ref}_{0,4}$, $\gamma_{0.7,4}$, m_4, $K_{0,4}$) for the pile load-movement curve and the load distribution over depth using the in situ load test data of bored pile A3. The optimized parameters, given in Table 4, are adopted in the simulations and the results are presented in Fig. 16. In all layers, the correlation of E^{ref}_{50} and E^{ref}_{ur} with E^{ref}_{oed} is taken into consideration. However, in contrast to the ranges given in Table 2, in this optimization, the dilation angle of each layer was directly linked to the corresponding friction angle by following $\psi_i = \max(\phi'_i - 30°, 0°)$. In this way, more appropriate combinations of dilation and friction angle could be guaranteed. Results for pile A3 indicate an improvement

Table 4
Optimized model parameters for the BEST.xmllabelt0020

Parameter Unit	γ_{sat} [kN/m^3]	ϕ' [°]	ψ_{max} [°]	E^{ref}_{oed} [MPa]	E^{ref}_{50} [MPa]	E^{ref}_{ur} [MPa]	m [-]	G^{ref}_0 [MPa]	$\gamma_{0.7}$ [-]	K_0 [-]
Layer L1	19.0	34.5	4.5	41.1	41.1	123.3	0.5	225.3	1.0E-4	0.66
Layer L2	16.0	26.0	0.0	4.8	6.0	30.0	0.9	93.4	1.9E-4	0.76
Layer L3	16.0	31.0	1.0	9.4	9.4	37.6	0.7	103.3	1.5E-4	0.63
Layer L4	19.0	37.0	7.0	25.0	25.0	75.0	0.5	159.1	1.3E-4	0.63
Layer L5	18.0	30.0	0.0	14.5	18.1	90.6	0.8	123.7	1.4E-4	1.28

black: optimized values, gray: average values

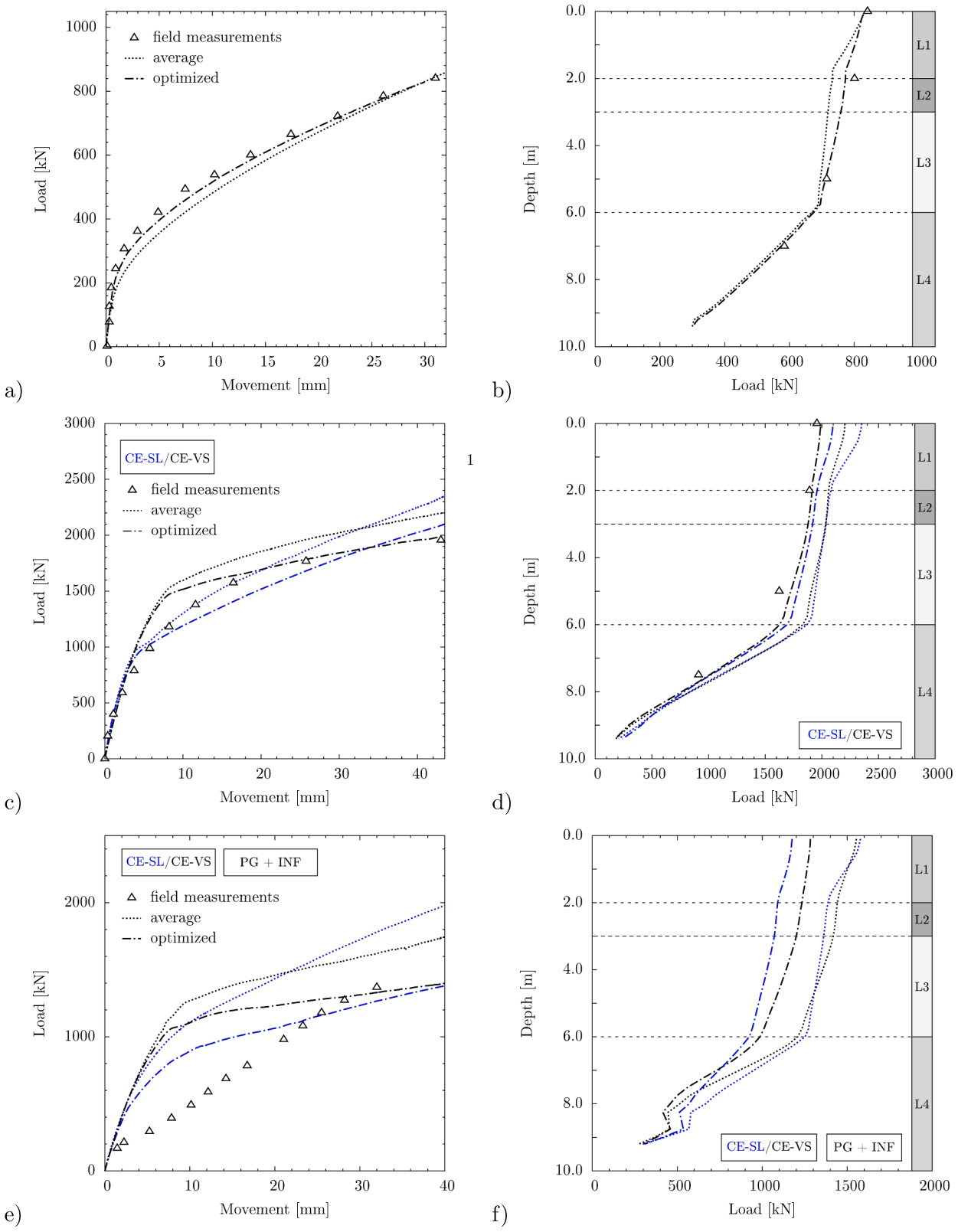

Fig. 16. Comparison of (left) load-movement curve and (right) load distribution over depth at 30 mm, 43.5 mm and 25 mm head movement for (a,b) a bored pile of 620 mm, (c,d) a full-displacement pile of 450 mm and (e,f) a full-displacement pile of 300 mm with attached expander body, respectively, using the average and optimized material parameter sets.

in the prediction of the pile response based on field measurements. This is consistent with the fact that the optimization procedure was undertaken to provide a better fit for the bored pile simulation against the reported field test.

Numerical simulation results of the FDP presented in Section 4.2 suggest that CE-SL and CE-VS approaches yield more accurate predictions compared to MEN and CE approaches. Hence, those two approaches are again pursued to assess the updated load-movement and

load distribution curves for the optimized set of parameters, as shown in Fig. 16(c) and (d), respectively. Comparing the load-movement curves obtained from the average and optimized parameters to those from field tests, one can conclude that while over-predicting the load capacity at pile head movements between 4 and 12 mm, CE-VS approach best resembles the field test measurements at pile C2 given the optimized parameter set is used. This statement can also be verified by looking at the load distribution results. Although a relatively better predicted load-movement response can be observed for CE-SL approach at pile head movements smaller than 10 mm, the load-movement response at larger movements as well as the load distribution response seems not to yield results as compared to field measurements as CE-VS approach.

Numerical simulation results for the FDP with attached EB, pile E1, are summarized in Fig. 16(e,f) and compared with field test results for the load-movement curve [Fig. 16(e)]. As previously discussed in Section 4.3, the linear load-movement response obtained from field measurements is believed to have been caused due to a lack of full initial contact between the pile tip and the soil below. Such detail is too complex to be precisely assessed and simulated in a numerical model. Therefore, the aim here is to best capture the pile load-bearing capacity at relatively large pile tip movements (e.g., >25 mm). Using the optimized parameter set and the earlier mentioned numerical simulation approaches for FDP and EB, the results shown in Fig. 16(e) indicate that both CE-SL and CE-VS approaches combined with Post Grouting (PG) and expander body INFlation (INF) techniques can provide acceptable load-bearing capacity estimation at relatively large pile tip movements.

6. Conclusion

Numerical analyses have been conducted to examine various methods to simulate head-down loading tests for bored piles, full-displacement piles, and full-displacement piles with attached expander body. Constitutive parameters derived from empirical correlations for the Bolivian Site for Testing piles (BEST) piles have been utilized to model the soil strata. Results have been compared with load test monitoring data of BEST in terms of load-movement response and load distributions along the pile. Furthermore, sensitivity analysis has been applied to identify the most relevant constitutive parameters, and inverse analysis has been utilized to fine-tune the simulations. Based on the analyses performed in the current study, the following general conclusions can be made:

1. Pile load-movement behavior is highly dependent on the relevance of the numerical simulation method and the reliability of soil parameters. It is observed that conservative, average, and optimistic estimates of the constitutive parameters derived via empirical correlations and stochastic analysis vary significantly. Using the average material parameter set, comparable predictions of the field measurements were achieved for piles A3 and C2, whereas the prediction for pile E1 was not found to have satisfactorily captured the field measurements.
2. Load distributions along the pile suggested that the shaft friction within the top soil layer was overestimated significantly. Since stresses are relatively small at shallow depths and field measurement instruments might not be in full contact with the soil to give accurate results, interpretations from empirical correlations to estimate soil parameters in the top few meters should be used with caution, as they might result in overestimation.
3. For the case of BEST, determination of installation effects for full-displacement piles using ICP design method (and other analytical CPT based design methods) leads to an underestimation of radial stresses and, thus, shaft resistance. Since ICP design method is applied in MEN method to determine radial stresses, shaft resistance has been under-predicted in this approach. A possible explanation for this observation may be that the design methods have been calibrated for sandy and not for silty or clayey soils.
4. Modeling the installation effects due to full-displacement piles using numerical approaches, such as the cavity expansion approach with vertical shearing (CE-VS) and the cavity expansion approach with sub layering (CE-SL), proved to give reasonable results for the full-displacement pile as well as for the full-displacement pile with attached expander body.
5. Comparison of results for full-displacement pile with attached expander body indicated that simulation of expander body installation effect is well captured via cavity expansion and base preloading to approximate the inflation and post grouting procedure, respectively.
6. Sensitivity analysis showed that the pile load-movement behavior is most sensitive to the friction angle, the primary compression stiffness and the lateral earth pressure coefficient of the layer in which the majority of pile length and its tip is located. In the case of the present study, such layer was in contact with 37% of the pile shaft and extended 3.5 m below the pile tip.
7. Comparison of optimized and average parameters revealed that the inverse analysis, in general, improved the results slightly. However, significant improvements could be observed for load distributions over pile depth for all piles under investigation, even though determination of the optimized parameters was solely based on the bored pile load test.

CRediT authorship contribution statement

Christoph Schmüdderich: Conceptualization, Methodology, Software, Validation, Data curation, Writing - review & editing, Visualization. **Mohammad Mahdi Shahrabi:** Conceptualization, Methodology, Investigation, Validation, Data curation, Writing - review & editing, Visualization. **Mahdi Taiebat:** Conceptualization, Methodology, Project administration, Supervision, Writing - review & editing. **Arash Alimardani Lavasan:** Conceptualization, Methodology, Project administration, Supervision, Writing - review & editing.

Declaration of Competing Interest

The authors declare that they have no known competing financial interests or personal relationships that could have appeared to influence the work reported in this paper.

Acknowledgments

The authors would like to express their sincerest reverence to Professor Tom Schanz, who passed away during this research, for his excellent scientific contributions and lasting memories.

References

Alawneh, A.S., Malkawi, A.H., 2000. Estimation of post-driving residual stresses along driven piles in sand. Geotech. Test. J. 23 (3), 313–326.
Baldi, G., Bellotti, R., Ghionna, V., Jamiolkowski, M., Marchetti, S., 1986. Pasqualini E., Flat dilatometer tests in calibration chambers. In: Proceedings of In Situ '86, ASCE Special Conference on 'Use of In Situ Tests in Geotechn. Engineering', pp. 431–446.
Basu, P., Prezzi, M., Salgado, R., 2013. Modeling of installation and quantification of shaft resistance of drilled-displacement piles in sand. Int. J. Geomech. 14 (2), 214–229.
Benz, T., 2007. Small-strain stiffness of soils and its numerical consequences. Univ. Stuttgart, Inst. f. Geotechnik Stuttgart, vol, 5.
Benz, T., Schwab, R., Vermeer, P., 2009. Small-strain stiffness in geotechnical analyses. Bautechnik 86 (S1), 16–27.
Berggren, B., Sellgren, E., Wetterling, S., 1998;;Report. Expanderkroppar. Anvisningar för dimensionering, utförande och kontroll (Expander Body. Instructions for design, installation and control). Swedish Commission on Pile Reseach 79, 1–54.
Bolton, M.D., 1986. The strength and dilatancy of sands. Geotechnique 36 (1), 65–78.
Briaud, J.L., Tucker, L., 1984. Piles in sand: a method including residual stresses. J. Geotech. Eng. 110 (11), 1666–1680.
Buljak, V., 2011. Inverse analyses with model reduction: proper orthogonal decomposition in structural mechanics. Springer Science & Business Media.
Chow, F., 1997. Investigations into displacement pile behaviour for offshore foundations. Ph D Thesis. Univ of London (Imperial College).

Clerc, M., 2013. Particle Swarm Optimization. John Wiley & Sons.
Dijkstra, J., Broere, W., Heeres, O., 2011. Numerical simulation of pile installation. Comput. Geotech. 38 (5), 612–622.
Engin, H., Brinkgreve, R., Van Tol, A., 2015. Simplified numerical modelling of pile penetration–the press-replace technique. Int. J. Numer. Anal. Meth. Geomech. 39 (15), 1713–1734.
Fellenius, B., Terceros, H. 2017. Information on the single pile, static loading tests at B.E. S.T. In: Proceedings of the 3rd Bolivian International Conference on Deep Foundations. p. 1–6.
Hamann, T., Qiu, G., Grabe, J., 2015. Application of a coupled eulerian–lagrangian approach on pile installation problems under partially drained conditions. Comput. Geotech. 63, 279–290.
Han, F., Salgado, R., Prezzi, M., Lim, J., 2017. Shaft and base resistance of non-displacement piles in sand. Comput. Geotech. 83, 184–197.
Jamiolkowski, M., LoPresti, D.C.F., M M.. 2001. Evaluation of relative density and shear strength of sands from cone penetration test and flat dilatometer test. ASCE Geotechnical Special Publication 119:201–238.
Jardine, R., Chow, F., Overy, R., Standing, J., 2005. ICP design methods for driven piles in sands and clays.
Jardine, R., Standing, J., Chow, F., 2006. Some observations of the effects of time on the capacity of piles driven in sand. Géotechnique 56 (4), 227–244.
Jardine, R.J., Merritt, A.S., Schroeder, F.C., 2015. The icp design method and application to a north sea offshore wind farm. In: IFCEE 2015pp. 247–256.
Johnston, I.W., Lam, T.S., 1989. Shear behavior of regular triangular concrete/rock joints–analysis. J. Geotech. Eng. 115 (5), 711–727.
Karlsrud, K., Clausen, C., Aas, P., 2005. Bearing capacity of driven piles in clay, the ngi approach. In: Proceedings of Int. Symp. on Frontiters in Offshore Geotechnics, Perth. p. 775–782.
Khaledi, K., Miro, S., König, M., Schanz, T., 2014. Robust and reliable metamodels for mechanized tunnel simulations. Comput. Geotech. 61, 1–12.
Knabe, T., Schweiger, H.F., Schanz, T., 2012. Calibration of constitutive parameters by inverse analysis for a geotechnical boundary problem. Can. Geotech. J. 49 (2), 170–183.
Ko, J., Jeong, S., Lee, J.K., 2016. Large deformation fe analysis of driven steel pipe piles with soil plugging. Comput. Geotech. 71, 82–97.
Krasiński, A., 2014. Numerical simulation of screw displacement pile interaction with non-cohesive soil. Arch. Civil Mech. Eng. 14 (1), 122–133.
Labenski, J., Moormann, C., 2016. A parametric study of different analytical design methods to determine the axial bearing capacity of monopiles. Geomech. Energy Environ. 6, 70–80.
Lee, J., Salgado, R., Carraro, J.A.H., 2004. Stiffness degradation and shear strength of silty sands. Can. Geotech. J. 41, 831–843.
Lee, J., Eun, J., Lee, K., Park, Y., Kim, M., 2008. In-situ evaluation of strength and dilatancy of sands based on cpt results. Soils Found. 48 (2), 255–265.
Lehane, B., Schneider, J., Xu, X., 2005. The UWA-05 method for prediction of axial capacity of driven piles in sand. Frontiers in offshore geotechnics. ISFOG 683–689.
Lorenzo, R., da Cunha, R., Cordão, Neto M., Nairn, J., 2017. Numerical simulation of installation of jacked piles in sand using material point method. Can. Geotech. J. 55 (1), 131–146.
Marchetti, S., 1980. In situ tests by flat dilatometer. ASCE J. Geotech. Eng. Division 106, 299–321.
Marchetti, S., Monaci, P., G T., M.C.. The Flat Dilatometer Test (DMT) in soil investigations. Tech. Rep.; International Society for Soil Mechanics and Geotechnical Engineering (ISSMGE); 2001.
Massarsch, K., Wetterling, S., 1993. Improvement of augercast pile performance by expander body system. In: 2nd International Seminar on Deep Foundations on Bored and Auger Piles, Ghent. p. 417–428.
McKay, M.D., Beckman, R., Conover, W., 1979. A comparison of three methods for selecting values of input variables in the analysis of output from a computer code. Technometrics Am. Stat. Assoc. 21, 239–245.
Miro, S., Hartmann, D., Schanz, T., 2014. Global sensitivity analysis for subsoil parameter estimation in mechanized tunneling. Comput. Geotech. 56, 80–88.
Müller, A.A., Messac, A., 2005. Extended radial basis functions: more flexible and effective metamodeling. AIAA J. 43 (6), 1306–1315.
Niazi, F.S., Mayne, P.W., 2013. Cone penetration test based direct methods for evaluating static axial capacity of single piles. Geotech. Geol. Eng. 31 (4), 979–1009.
Phuong, N., Van Tol, A., Elkadi, A., Rohe, A., 2016. Numerical investigation of pile installation effects in sand using material point method. Comput. Geotech. 73, 58–71.
Pucker, T., Grabe, J., 2012. Numerical simulation of the installation process of full displacement piles. Comput. Geotech. 45, 93–106.
Rooz, A.F.H., Hamidi, A., 2019. A numerical model for continuous impact pile driving using ale adaptive mesh method. Soil Dyn. Earthquake Eng. 118, 134–143.
Said, I.D., De Gennaro, V., Frank, R., 2009. Axisymmetric finite element analysis of pile loading tests. Computers Geotech. 36 (1), 6–19.
Sakurai, S., Akutagawa, S., Takeuchi, K., Shinji, M., Shimizu, N., 2003. Back analysis for tunnel engineering as a modern observational method. Tunn. Undergr. Space Technol. 18 (2–3), 185–196.
Saltelli, A., Ratto, M., Andres, T., Campolongo, F., Cariboni, J., Gatelli, D., et al., 2008. Global Sensitivity Analysis: The Primer. John Wiley & Sons.
Schanz, T., Vermeer, P., Bonnier, P.,1999. The hardening soil model: formulation and verification. Beyond 2000 in computational geotechnics. pp. 281–296.
Sobol, I.M., 1993. Sensitivity estimates for nonlinear mathematical models. Math. Modell. Comput. Exp. 1 (4), 407–414.
Terceros, M.A., Massarsch, K.R. 2014. The use of the expander body with cast in situ piles in sandy soils. In: DFI/EFFC International Conference on Piling and Deep Foundations. Stockholm, Sweden. p. 347–358.
Terceros Herrera, M., Wetterling, S., Massarsch, K., 1995. Application of the soilex pile system with expander body in bolivia. In: Proc. of 10th. Congreso Panamericano de Mecánica de Suelos e Ingeniería de Cimentaciones, Guadalajara, Mexico. p. 1319–1327.
Wehnert, M., Vermeer, P., 2004. Numerical analyses of load tests on bored piles. Numerical methods in geomechanics–NUMOG IX. pp. 505–511.
Xu, X., Schneider, J.A., Lehane, B.M., 2008. Cone penetration test (CPT) methods for end-bearing assessment of open-and closed-ended driven piles in siliceous sand. Can. Geotech. J. 45 (8), 1130–1141.
Yazdani, M., Sharifzadeh, M., Kamrani, K., Ghorbani, M., 2012. Displacement-based numerical back analysis for estimation of rock mass parameters in siah bisheh powerhouse cavern using continuum and discontinuum approach. Tunn. Undergr. Space Technol. 28, 41–48.
Zhao, C., Lavasan, A.A., Barciaga, T., Zarev, V., Datcheva, M., Schanz, T., 2015. Model validation and calibration via back analysis for mechanized tunnel simulations–the western scheldt tunnel case. Comput. Geotech. 69, 601–614.
Zhao, C., Lavasan, A.A., Hölter, R., Schanz, T., 2018. Mechanized tunneling induced building settlements and design of optimal monitoring strategies based on sensitivity field. Comput. Geotech. 97, 246–260.